Check for updates

Characterization of Upper Cretaceous Matulla and Wata clastic reservoirs from October field, Central Gulf of Suez, Egypt

Sherif Farouk · Souvik Sen · Saada Ahmed Saada · Ahmed M. Eldosouky ·
Romaisaa Elsayed · Ahmed A. Kassem · Khaled Al-Kahtany ·
Ahmed Abdeldaim

Abstract The objective of this study was to integrate petrographic thin sections, SEM, XRD, routine core analysis, gas chromatography, and wireline logs to present a comprehensive petrographic and petrophysical assessment of the shallow marine clastic reservoirs of the Coniacian-Santonian Matulla Formation and upper Turonian Wata Formation from the October field, Central Gulf of Suez Basin. The fine to very fine-grained glauconite-bearing subarkose quartz arenites of the Matulla and Wata reservoirs exhibit good intergranular primary porosity with good pore connectivity. Moderate to slight compaction and grain to grain pressure solution resulted in a slightly inhomogeneous packing of framework grains.

Feldspar dissolution contributed to the secondary porosity which improved the reservoir quality, while quartz overgrowth and minor calcite cementation are inferred as porosity destroying diagenetic agents. Pore-filling kaolinite and clay phases also had a negative effect on reservoir storage capacity. Routine core analysis indicated > 20% porosity and up to 412 mD permeability in the meso-megaporous sandstones of both the reservoirs. Permeability anisotropy analysis of Matulla samples indicates the dominance of primary depositional fabric and isotropic pores with minor scattered/connected horizontal pores and vertical pore connectivity. Wireline log-based quantitative petrophysical assessments exhibit low shale volume

S. Farouk (✉)
Exploration Department, Egyptian Petroleum
Research Institute (EPRI), 1 Ahmed El-Zomor Street,
Nasr City 11727, Cairo, Egypt
e-mail: geo.sherif@hotmail.com

S. Sen
Geologix Limited, Dynasty Building, Wing A,
Level 4, Andheri Kurla Road, Andheri (E), Mumbai,
Maharashtra 400059, India

Present Address:
S. Sen
Reservoir Technical Services (RTS), Baker Hughes,
Mumbai, India

S. A. Saada · A. M. Eldosouky · R. Elsayed
Geology Department, Faculty of Science, Suez University,
Suez 43518, Egypt

A. A. Kassem
Exploration Department, Gulf of Suez Petroleum
Company, New Maadi 11742, Cario, Egypt

K. Al-Kahtany
Geology and Geophysics Department, College of Science,
King Saud University, 11362 Riyadh, Saudi Arabia

A. Abdeldaim
Faculty of Earth Science and Engineering, University
of Miskolc, Miskolc 3515, Hungary

A. Abdeldaim
Geology Department, Faculty of Science, South Valley
University, Qena 83523, Egypt

🖄 Springer

and higher hydrocarbon saturation (up to 80%) on both the reservoirs, which is also supported by the gas chromatography data confirming the presence of oil in the Matulla, and Wata pay zones based on interpreted gas balance, wetness, and character ratios. The study concludes excellent reservoir properties in the Upper Cretaceous clastic intervals of the October field.

Highlights

- Matulla and Wata reservoirs consist of meso-megaporous glauconitic subarkose quartz arenites.
- Feldspar dissolution, calcite cementation and quartz overgrowth are inferred as principal diagenetic factors controlling reservoir quality.
- Gas chromatography data confirms the presence of oil in Matulla and Wata reservoirs.
- Both reservoirs exhibit primary and secondary porosity, good permeability, and high hydrocarbon saturation in the pay zones.

Keywords Petrography · Core analysis · Petrophysics · Matulla · Wata · Gulf of Suez

1 Introduction

The Gulf of Suez sedimentary rift basin, with aerial coverage of around 19,000 km^2, is the most prolific hydrocarbon provincial basin of Africa. It is delineated on both margins by large-scale NW-striking normal fault zones that define half-grabens (Jackson et al. 2006). The basin is developed as a result of the separation of the Arabian plate from the African plate. The basin hosts more than eighty hydrocarbon fields established based on 240 discoveries made from thousands of exploratory well drilling and these finds include up to 1 million bbl in the Precambrian-Quaternary reservoirs (Wescott et al. 2016), and thus of great interest to the Egyptian upstream industries (e.g., Alsharhan 2003). Recent discoveries in the Abu Rudeis Sidri development lease by ENI (2019) and Ramadan region by Dragon Oil (JPT 2022) had attracted the upstream community and rejuvenates the oil and gas exploration activities in the Gulf of Suez. The Gulf of Suez is structurally complex, and

the new plays and untapped hydrocarbon pools can be accessed with new technological advancements (i.e., seismic imaging, drilling complex geometries etc.). Structural and property (facies and petrophysical) modeling are important can enhance the subsurface understanding of the potential reservoir intervals as well as producing reservoirs, that directly affects the forthcoming field development strategies, future well placements etc. (El-Gendy et al. 2017a, b, 2022; Nabawy and Barakat 2017; Barakat et al. 2022; Nabawy et al. 2022).

The present study focuses on the Upper Cretaceous sandstones of the October field from the Central Gulf of Suez Basin. The field started producing in 1977 and reached a time of peak production of 136,000 BOPD (barrels of oil per day) (Askar et al. 2020). Along with the Nubia sandstones, the upper Turonian Wata Formation and Coniacian-Santonian Matulla Formation of the Nezzazat Group formed key reservoirs in the October field (Lelek et al. 1992). Nezzazat reservoirs were developed later when Nubia was depleted (Hassan et al. 2006). The latest published production figure from the October field stands at 16,000 BOPD with high water cut (Noureldien and Nabil 2016).

Reservoir completion and production-related aspects are well published from the October field (Borling et al. 1996; Ibrahim et al. 1999; Hassan et al. 2006; Ibrahim et al. 2008; Nassar and Noureldien 2013; Askar et al. 2020). El-Ghamri et al. (2002) presented the oil generation and migration aspects. Sercombe et al. (1997, 2012) and Gawad et al. (2021b) interpreted the structural geology of the field and reservoir modeling aspects. Lashin and Mogren (2012) and Gawad et al. (2021a) characterized the source rock properties and analyzed the petroleum system of the October field. Kassem et al. (2020) studied the organic geochemical and isotope data of the Cenomanian–Turonian shales and limestones from the October field and linked the sediments with oceanic anoxic event 2 (OAE2) which produced organic-rich intervals. Kassem et al. (2021) inferred the geomechanical characteristics of the Cretaceous Nezzazat and Paleozoic Nubia reservoirs to infer the influences of fluid injection and depletion on reservoirs' geomechanical stability and field development. Kassem et al. (2022) presented a microfacies analysis of the Wata Formation and inferred intertidal /shelf depositional settings.

Other works from the Nezzazat Group from the Central and Southern Gulf of Suez includes the analysis of reservoir geometry (Hasouba et al. 1992), glauconite effects on logs (El Bahr et al. 1992), lithology evaluation (Marttila and El Bahr 1994) and petrophysical rock typing of Matulla Formation (El Sharawy and Nabawy 2016). A detailed petrographic, diagenetic and petrophysical investigation of the Matulla and Wata clastic reservoirs from the October oil field are lacking in the literature, which have been the primary objective of our study. In this work, we have combined thin section petrography, X-ray diffraction (XRD), scanning electron microscopy (SEM), routine core analysis (RCAL), wireline logs and gas chromatography data to assess the reservoir properties of the Upper Cretaceous Matulla and Wata sandstone reservoirs from the October oil field, such integrated analysis were not attempted before. Principal objectives

of the study include: (i) petrographic characteristics and rock constituents, (ii) diagenetic features, (iii) porosity and permeability distribution, (iv) permeability anisotropy, (v) wireline log-based quantitative petrophysical assessment and (vi) hydrocarbon characteristics based on gas chromatography data. Results have been discussed and inferences are drawn on the effect of diagenesis on reservoir properties.

2 Geological settings

The Gulf of Suez is a shallow, slightly arcuate, northwest-southeast-trending depression that is defined by longitude 32°10' and 34°E and latitude 27° and 30°N (Fig. 1). It forms an elongated graben with a length of around 320 km, a breadth of 30–80 km, and a sea depth of 40–60 m. The separation between Arabian

Fig. 1 Location of the studied field in the central Gulf of Suez Basin, as marked by red polygon. The structural trends are adapted from El-Gendy et al. (2017a)
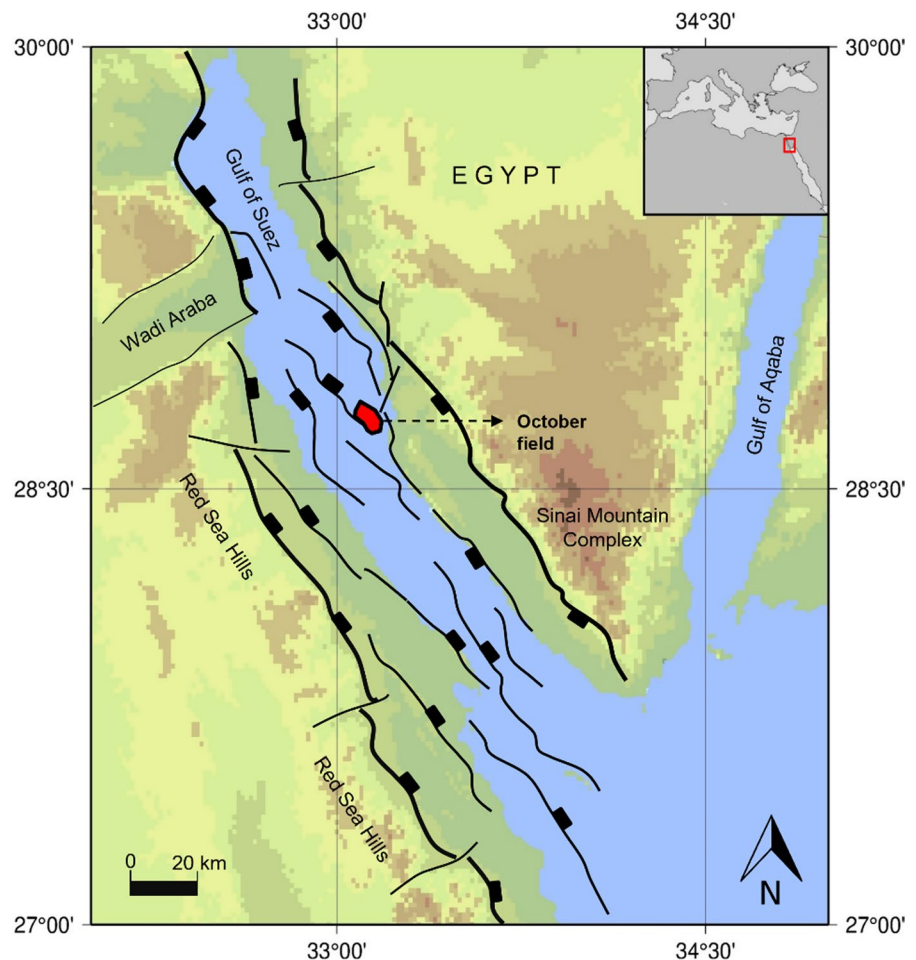
and African plates during Cenozoic created this rift basin (Hempton 1987; Meshref 1990; Makris and Henke 1992; La Brecquet and Zitellini 1985). Rifting started in the late Oligocene to early Miocene, and continued until the late Miocene (Bosworth et al. 2020). The southern Suez rift ends by creating a triple junction with Gulf of Aqaba and Red Sea rifting. Meshref (1990) subdivided the Suez rift basin into various structural provinces based on dip variations within large fault blocks constituting of eroded horsts and deep grabens. The October Field is positioned in the central Gulf of Suez (Fig. 1) (EGPC 1996). An NNE striking cross fault divided the field into two main fault compartments with the northern compartment being at the down thrown side. The pre-rift stratigraphy displays a relatively uniform dip towards NE. The overlying Lower Miocene beds also dip to the NE.

Figure 2 presents the lithostratigraphic succession of the October oil field, based on the interpreted and correlated formation tops from the four studied wells. Three major lithostratigraphic units classified the successions according to rifting events with different thicknesses and facies characteristics are: post-rift (post-Miocene), Miocene syn-rift, and pre-rift (ranging between Upper Eocene and Pre-Cambrian). The pre-rift mixed clastic and carbonate stratigraphy was deposited in terrestrial, shallow marine or marginal marine environments which were differentiated by non-depositional/erosional unconformities. The pre-rift sediments exhibit highly heterogeneous distribution laterally with minimum thickness being reported in the southern region and highest thickness in the central province. The Late Cretaceous stratigraphy is classified into the Cenomanian Raha Formation, overlain by Turonian Wata Formation and the Coniacian–Santonian Matulla Formation, mostly of shallow marine origin (Hassouba et al. 1992). The variation in thickness of the Wata and Matulla formations is clearly observed in the Gulf of Suez, indicating tectonic activity after the deposition of the Turonian (Farouk 2015). These three units form the Nezzazat Group which is overlain by the Brown Limestone and Sudr Formations (Schütz 1994). Hydrocarbons in the October field are produced from four reservoir intervals: the Carboniferous-Lower Cretaceous Nubian Sandstones, the Upper Cretaceous Nezzazat Group, the Lower Miocene Nukhul Formation, and the Asl Member of the Lower Miocene Upper Rudeis

Formation (El-Ghamri et al. 2002). Based on numerous oil/source rock correlations, Abdine et al. (1992) concluded that the Brown Limestone Member of the mature Sudr Formation is the most probable source of oil in the October field. Middle Miocene regional uplift resulted in the Gulf of Suez becoming an enclosed basin with the deposition of extensive evaporites (Belayim, South Gharib and Zeit Formations) which provide a regional seal across the region (Abdine et al. 1992). The presence of trap-bounding faults and their sealing properties were reported to be critical for charging the October field and related structures (El-Ghamri et al. 2002).

3 Data and methods

We have studied the Upper Cretaceous Matulla and Wata reservoirs from four wells drilled in the October field, A-10, B-6, A-3, and G-11 (Fig. 3). All these four wells were drilled till Nubia Formation, which was the primary producer of the October field. The well A-3 and B-6 were drilled in 1981 and 1983, respectively, and both the wells are now in shut in phase. G-11 and A-10 were drilled in 1993 as development wells. Presently G-11 is oil producing and A-10 is being used as a water injector well. The Matulla Formation was encountered between 10,941–11,342 ft, 11,005–11,207 ft, 10,204–10,915 ft, and 10,385–10,797 ft in the wells A-10, B-6, A-3, and G-11, respectively. The Wata Formation was encountered between 11,342–11,688, 11,207–11,570, and 10,797–11,160 ft in the wells A-10, B-6, and G-11, respectively. In the well A3, the Wata Formation was absent, and Matulla Formation directly overlies the Raha Formation due to tectonic uplift and faulting. Both the formations host mixed siliciclastic and carbonate intervals; however, this study focuses on the sandstone reservoir zones of the mentioned formations. The formation thicknesses in all the studied wells are presented in Fig. 2. A well log correlation panel is presented in Fig. 4. Conventional cores were retrieved from the Matulla and Wata Formations from three wells, A-10, G-11, and A-3. Thin section petrography, SEM and XRD were performed on 6 Matulla samples and 8 Wata samples from the wells A-10 and G-11. These datasets are used to infer mineralogical distribution, texture, diagenetic
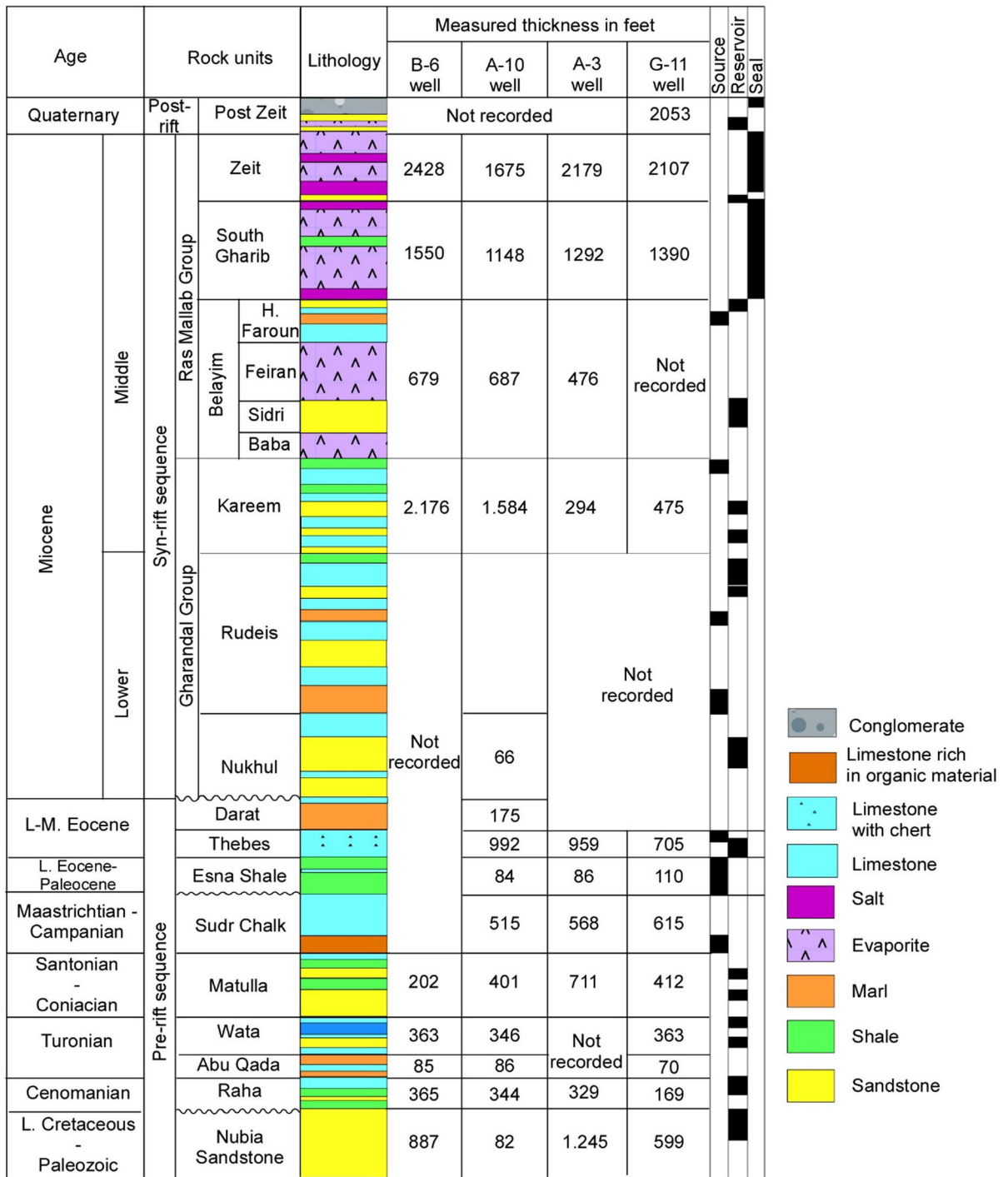
Age			Rock units		Lithology	Measured thickness in feet				Source	Reservoir	Seal
						B-6 well	A-10 well	A-3 well	G-11 well			
Quaternary		Post-rift	Post Zeit			Not recorded			2053			
Miocene		Syn-rift sequence — Ras Mallab Group	Zeit			2428	1675	2179	2107			
			South Gharib			1550	1148	1292	1390			
	Middle		Belayim	H. Faroun		679	687	476	Not recorded			
				Feiran								
				Sidri								
				Baba								
		Syn-rift sequence — Gharandal Group	Kareem			2.176	1.584	294	475			
	Lower		Rudeis						Not recorded			
			Nukhul			Not recorded	66					
L-M. Eocene		Pre-rift sequence	Darat				175					
			Thebes				992	959	705			
L. Eocene-Paleocene			Esna Shale				84	86	110			
Maastrichtian - Campanian			Sudr Chalk				515	568	615			
Santonian - Coniacian			Matulla			202	401	711	412			
Turonian			Wata			363	346	Not recorded	363			
			Abu Qada			85	86		70			
Cenomanian			Raha			365	344	329	169			
L. Cretaceous - Paleozoic			Nubia Sandstone			887	82	1.245	599			

Legend:
- Conglomerate
- Limestone rich in organic material
- Limestone with chert
- Limestone
- Salt
- Evaporite
- Marl
- Shale
- Sandstone

Fig. 2 Lithostratigraphic succession of the studied October oil field, Gulf of Suez Basin, Egypt based on the interpreted and correlated formation tops in the four studied wells. (Alsharhan 2003; El Diasty et al. 2020). This study focuses on the clastic reservoirs of the Matulla and Wata formations

Fig. 3 Location of the studied wells in the October field
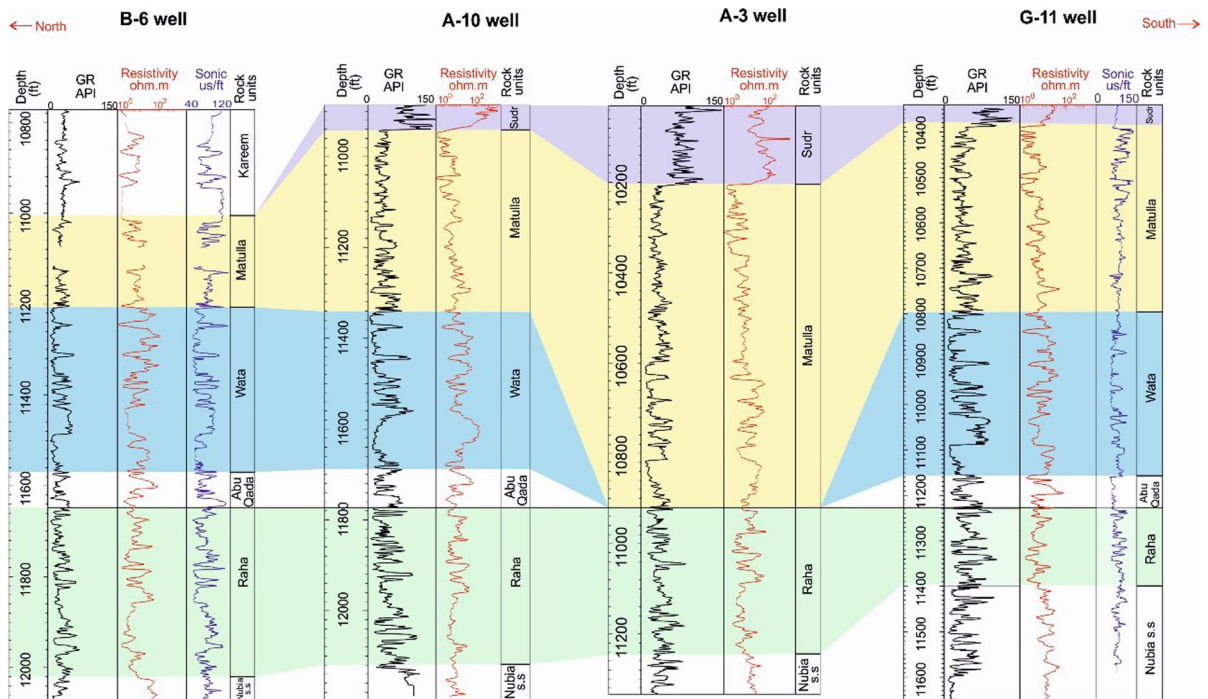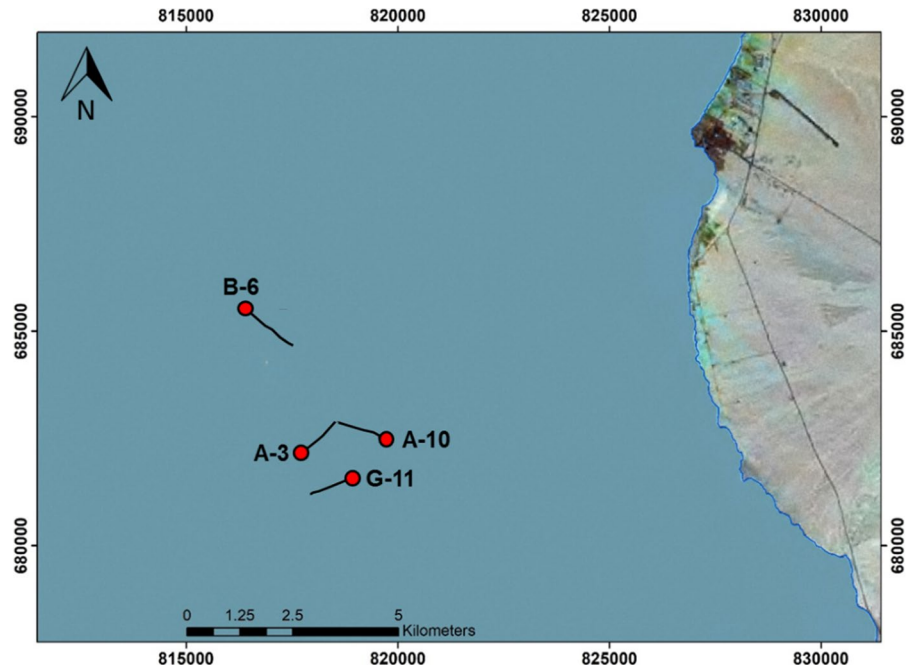

Fig. 4 Well log correlation panel using the four studied wells in the October oil field

effects, porosity types and clay mineral phases present within the studied reservoirs. Gas chromatography data was studied from the well A-10. Based on the total gas and chromatographs (C1–C5), following gas ratios were estimated (Haworth et al. 1985):

$$Wh = \left[\frac{C2 + C3 + C4 + C5}{C1 + C2 + C3 + C4 + C5} \right] *100 \qquad (1)$$

$$Bh = \frac{C1 + C2}{C3 + C4 + C5} \qquad (2)$$

$$Ch = \frac{C4 + C5}{C3} \qquad (3)$$

where Wh, Bh and Ch denote wetness, balance and character ratios, respectively. Based on the value ranges of the estimated gas ratios, reservoir fluid types are inferred (Haworth et al. 1985; Mode et al. 2014; Pierson 2017).

Routine core analysis provided direct measurements of porosity (Φ) and horizontal permeability (Kh) from 52 Matulla core plugs (46 measurements from the well A-3, 6 from G-11) and 6 Wata core plugs from A-10 and G-11. Vertical permeability (Kv) data was also available from the 46 Matulla plugs of the well A-3, which was utilized to infer the permeability anisotropy:

$$\lambda k = \sqrt{\frac{Kh}{Kv}} \qquad (4)$$

Wireline logs were recorded in all the wells, which were utilized for quantitative petrophysical interpretation. We determined the essential petrophysical parameters that include shale volume (Vsh, using gamma ray log), total and effective porosity (Φt and $\Phi e,$ respectively, using neutron porosity, density and Vsh), water saturation (Sw, using Indonesian model), and bulk volume of water (BVW) (Buckles 1965; Poupon and Leveaux 1971; Asquith and Gibson 1982). Pickett plot was constructed to infer the input parameter values for Sw estimation (Pickett 1973). Net reservoir pay interval was distinguished based on the petrophysical cut offs of Vsh = 0.35 v/v, $\Phi e = 0.1$ v/v and Sw = 0.5 v/v, as commonly reported from Gulf of Suez (Ali et al. 2022).

4 Results

4.1 Petrographic investigation

4.1.1 Matulla reservoir

Thin section analysis indicates that the Matulla sandstones are well to moderately sorted, mature, fine to very fine-grained, subrounded to subangular. Framework grains are predominantly quartz, feldspar, minor rock fragments along with well-rounded glauconite grains/peloids (Fig. 5). Moderate to slight compaction and grain to grain pressure solution results in a slightly inhomogeneous packing of framework grains. Leaching of feldspar, quartz cementation and overgrowths along with minor pyrites are commonly observed in all the Matulla thin sections (Fig. 5). Matrix consists predominantly of clayey pseudomatrix which results from the compaction/alteration of argillaceous rock fragments (Fig. 5). Pore-filling kaolinite clay forms as an alteration product of the pseudomatrix which resembles detrital matrix (Fig. 5). Calcite cementation is not common, it was observed in one of the thin sections (Fig. 5d). Primary intergranular porosity is dominant which exhibits good interconnectivity, indicated by blue dye impregnation in all the thin sections (Fig. 5). Dissolution of unstable framework grains produced secondary pores (Fig. 5a, c, d). Permeability is reduced due clayey pseudomatrix, pressure solution among quartz grains, and the discontinuous nature of the organic-rich, clayey lamina. SEM images indicated quartz framework grains with overgrowth and dominant intergranular porosities (Fig. 6). Pore-filling authigenic clay (Fig. 6a, b, d) and kaolinite booklets (Fig. 6c, d) are commonly observed along with minor calcite cements (Fig. 6d).

4.1.2 Wata reservoir

Thin section analysis indicates that the Wata sandstones are moderate-well sorted, mature, very fine- to fine-grained, subrounded to subangular, containing abundant clayey material (Fig. 7). Moderate compaction, pressure solution, quartz overgrowth cement, and calcite cement has given the rock a spotty "welded" appearance and resulted in a slight inhomogeneity of packing. Framework grains are predominantly quartz, feldspar, and lesser amounts of rock fragments. Minor
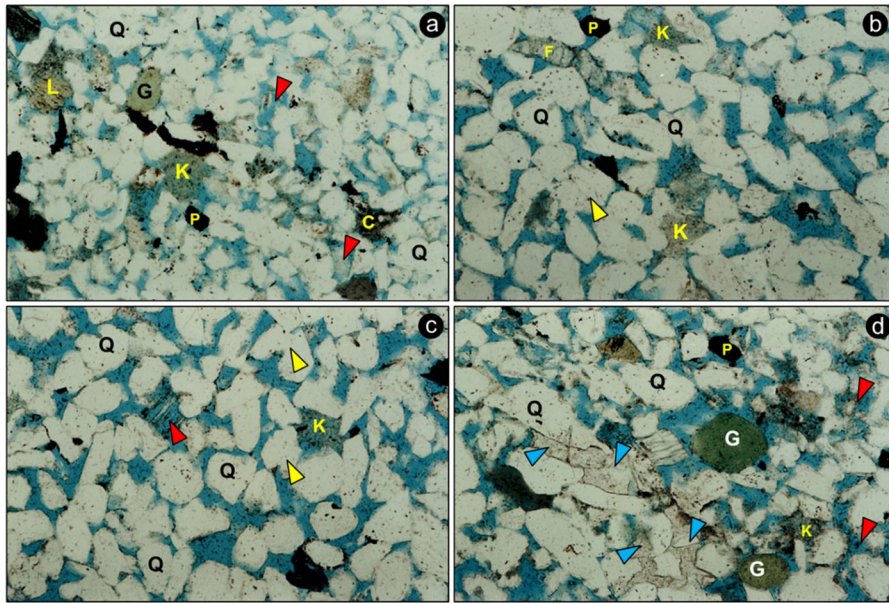
Fig. 5 Optical photomicrographs of Matulla sandstones under plane polar at **a** 10,716 ft, sample 11A, **b** 10,723 ft, sample 18A, **c** 10,732 ft, sample 27A, and **d** 10,773 ft, sample 53A from the well G-11, indicating subangular to subrounded quartz (Q), feldspar (F), minor rounded glauconite (G), illitic lithic fragments (L), pore-filling kaolinite (K), clayey pseudomatrix (C), pyrite (P), feldspar dissolution (red arrows), quartz overgrowth cementation (yellow arrows), pore-filling calcite cement (blue arrows). Intergranular porosity is represented by blue dye. Field of view is 1 mm

Fig. 6 SEM images of Matulla sandstones at **a** 10,723 ft, sample 18A, **b** 10,732 ft, sample 27A, **c** 10,777.5 ft, sample 57A, and **d** 10,773 ft, sample 53A from the well G-11, indicating quartz framework grains (Q) with intergranular porosities (green arrows), fine crystalline pore-filling authigenic clays (C), quartz overgrowth cementation (yellow arrows), pore-filling kaolinite (K), calcite cementation (blue arrow). Scale bar is 10 microns
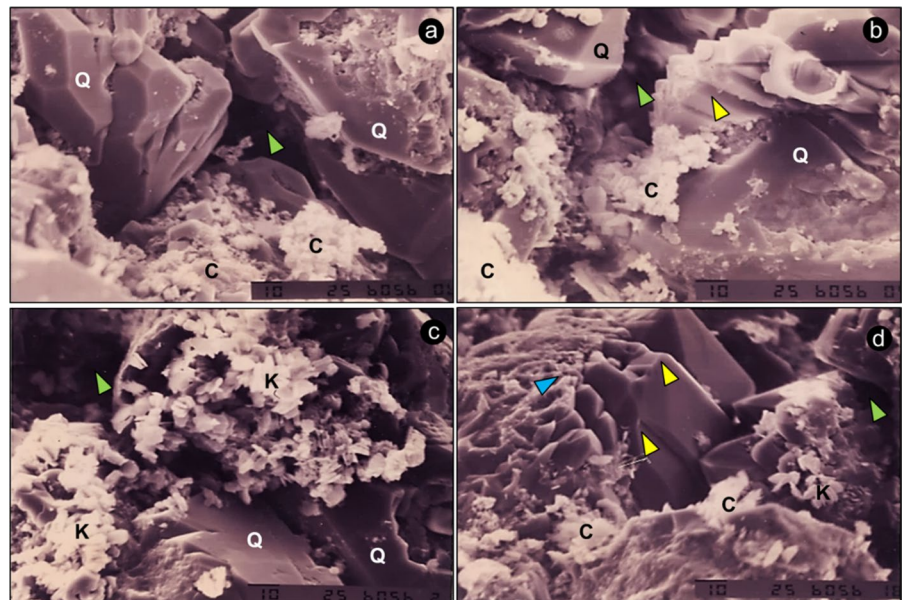
siderite is observed in few thin sections (Fig. 7a). Matrix consists predominantly of clayey pseudomatrix (Fig. 7b–d) which results from the compaction/alteration of argillaceous rock fragments. Some detrital clay is suspected as matrix due to the finely laminated texture of the rock, but it is often difficult to distinguish from pseudomatrix. Extensive feldspar leaching (Fig. 7a, c), quartz overgrowth cements
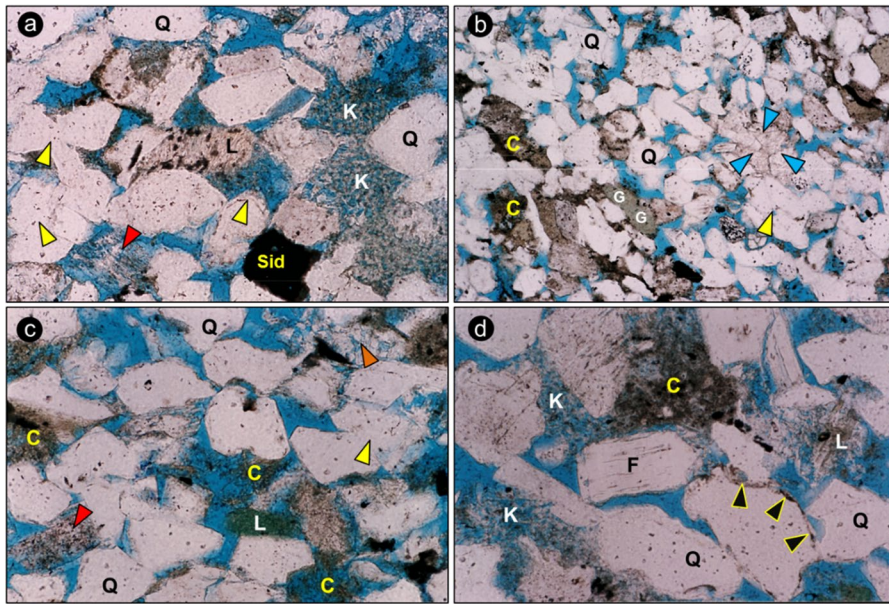
Fig. 7 Optical photomicrographs of Wata sandstones under plane polar at **a** 11,580.2 ft, sample 22A, Field of view is 0.5 mm, **b** 11,569.5 ft, sample 17A, Field of view is 1 mm, **c** 11,581.3 ft, sample 23A, and **d** 11,584.7 ft, sample 26A from the well A-10, indicating subangular to subrounded quartz (Q), feldspar (F), lithic fragments (L), minor rounded glau-conite (G), pore-filling kaolinite (K), clayey pseudomatrix (C), pyrite (P), feldspar dissolution (red arrows), quartz overgrowth cementation (yellow arrows), pore-filling calcite cement (blue arrows), chlorite rims surrounding quartz grains (black arrows), minor siderite (Sid). Intergranular porosity is represented by blue dye

Fig. 8 SEM images of Matulla sandstones at **a** 11,580.2 ft, sample 22A, **b** 11,569.5 ft, sample 17A, **c** 11,581.3 ft, sample 23A, and **d** 11,584.7 ft, sample 26A from the well A-10, indicating quartz framework grains (Q) with intergranular porosities (green arrows), feldspar (F) dissolution along the cleavage planes, alteration rim formed of chlorite (black arrows) defining relict grain, fine crystalline pore-filling authigenic clays (C), quartz overgrowth cementation (yellow arrows), pore-filling kaolinite booklets (K). Scale bar is 10 microns
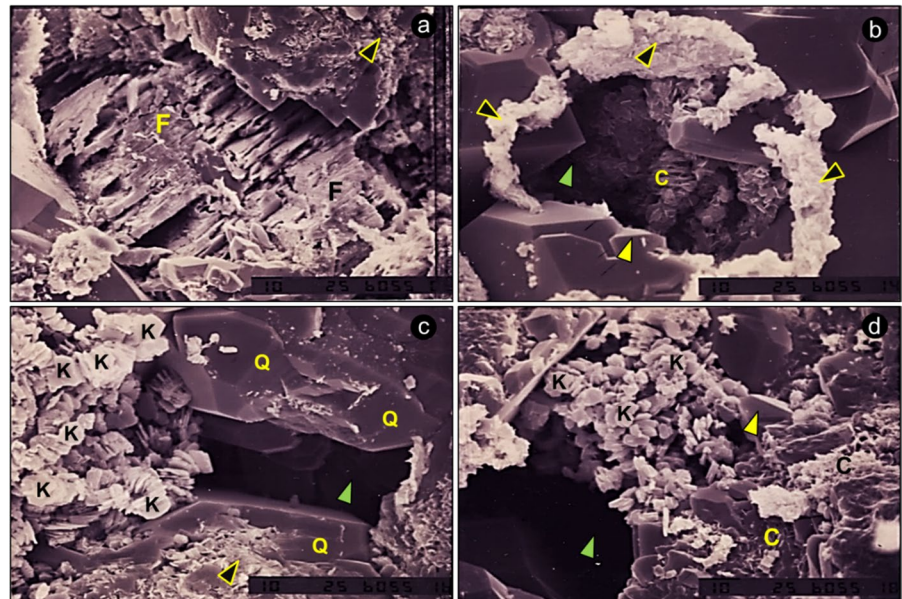
(Fig. 7a–c), pressure solution among quartz grains, authigenic kaolinite (Fig. 7a, c) and chloritization of argillaceous rock fragments (Fig. 7d) are commonly observed in the Wata thin sections. Pore system consists of primary intergranular porosity with good pore connectivity and feldspar dissolution-induced secondary porosity. SEM images indicated quartz framework grains with overgrowth and intergranular porosities (Fig. 8b–d). Dissolution of feldspar grains along the cleavage planes are observed in SEM (Fig. 8a) contributing to secondary porosity. SEM also reveals abundant pore-filling kaolinite booklets (Fig. 8c, d), authigenic clays (Fig. 8b, d) and alteration rims composed of chlorites (Fig. 8b).

4.1.3 XRD results

The XRD measurements from the Matulla samples of the well G-11 indicates quartz to be the most dominant mineral with abundance ranging between 69 and 95%, along with 1–7% total feldspar (average ~ 4%), minor siderite (0.5–1%) and pyrite (0–0.5%) (Fig. 9a). Based on the petrographic analysis, the studied Matulla and Wata reservoirs are classified as glauconitic subarkose quartz arenites, following the sandstone classification scheme provided by Dott (1964).

Carbonates are present in trace amounts, however one sample (no. 53A) exhibits ~ 5% calcite, which was also observed in the thin section (Fig. 5d) and SEM images (Fig. 6d) as pore filling cements. The total clay volume of the Matulla samples varies between 4 and 23%, which is composed of mostly kaolinite, chlorite, and mixed clay (illite/smectite) (Fig. 9b).

The Wata sandstone samples from the wells A-10 and G-11 also exhibits similar characteristics, with quartz being the most dominant mineral (60–83%) along with 6–13% feldspar (average ~ 8%) (Fig. 10a). Siderite and pyrite are present in trace quantities. Average clay volume in the eight samples is 18% (Fig. 10a), dominated by kaolinite and chlorite (Fig. 10b), as also seen in SEM images (Fig. 8b–d).

4.2 Petrophysical assessment

4.2.1 Routine core analysis

Porosity and permeability of the two studied reservoirs are inferred from direct core measurements from three wells, A-10, G-11, and A-3. The Matulla sandstones exhibit a wide porosity (4.5–27.1%) and horizontal permeability (0.03–170 mD) distribution indicating micro- to megaporosity (Fig. 11). The average
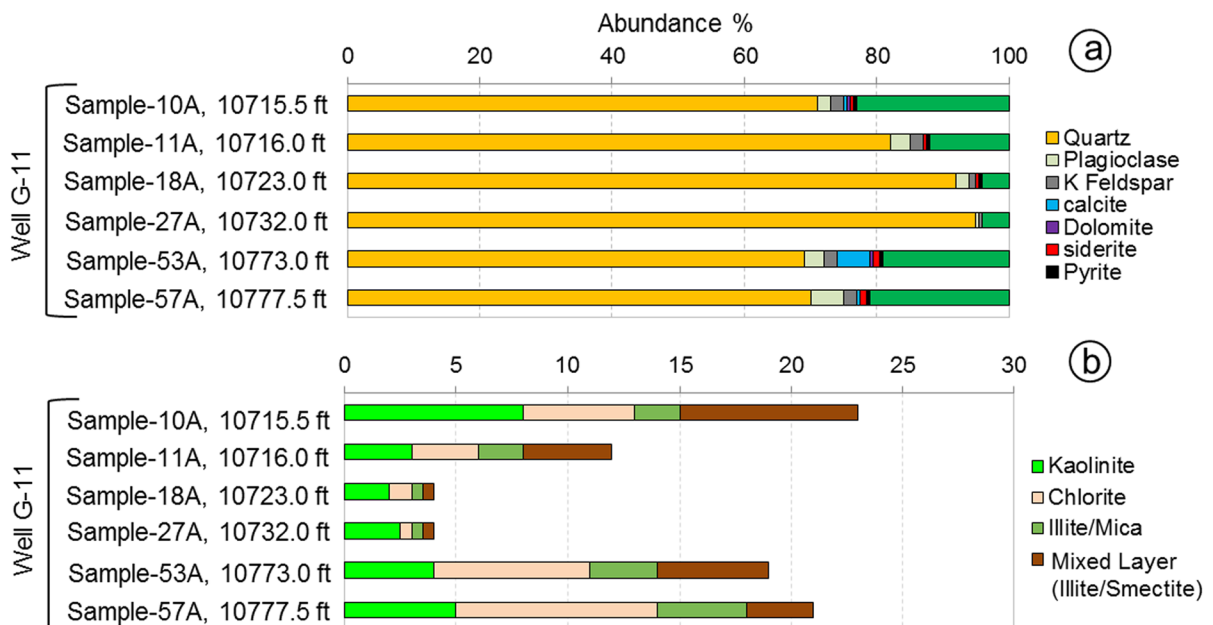

Fig. 9 XRD results of Matulla sandstone from the well G-11, indicating **a** mineral constituents and **b** clay fraction
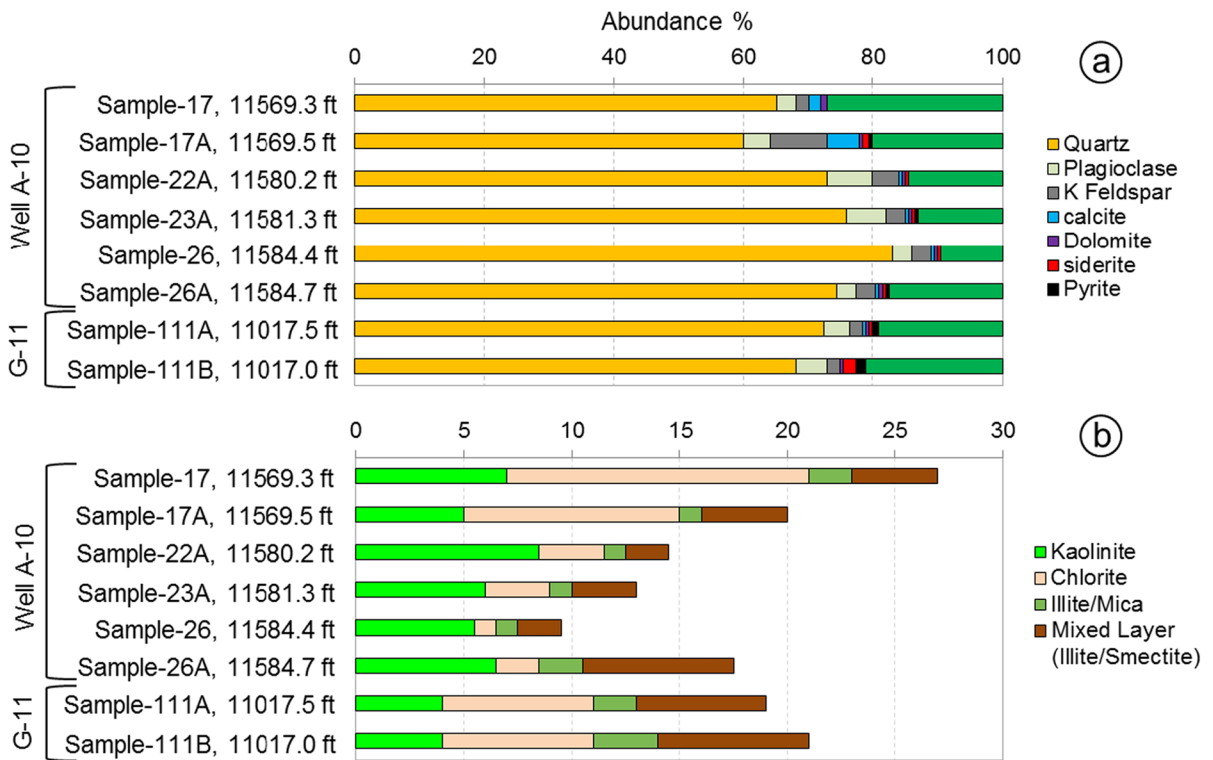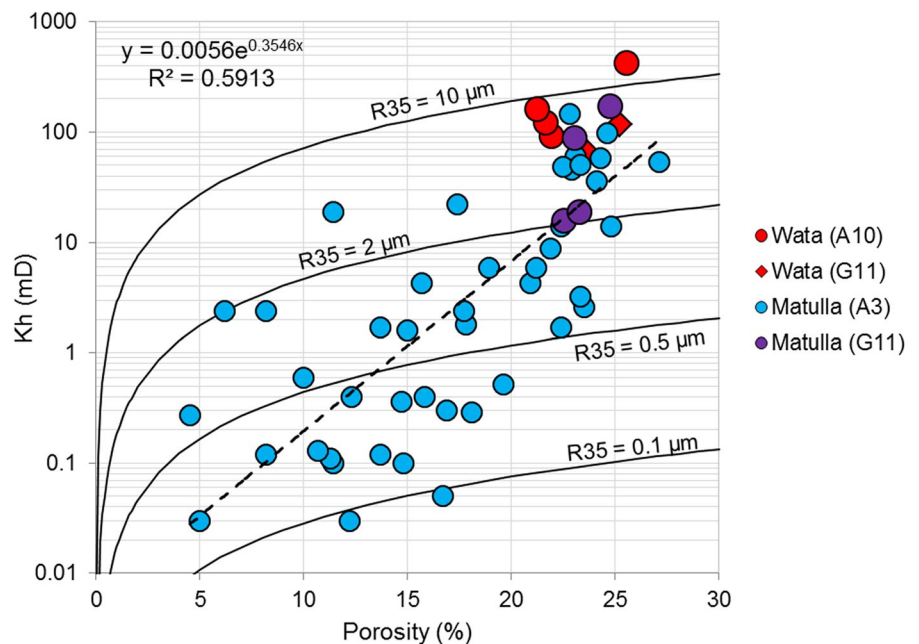
Fig. 10 XRD results of Wata sandstone from the wells A-10 and G-11, indicating **a** mineral constituents and **b** clay fraction

Fig. 11 Relationship between core-derived porosity and horizontal permeability (Kh) of the Matulla and Wata sandstone reservoirs from the October field. R35 denotes the pore throat radius (Kolodzie 1980)
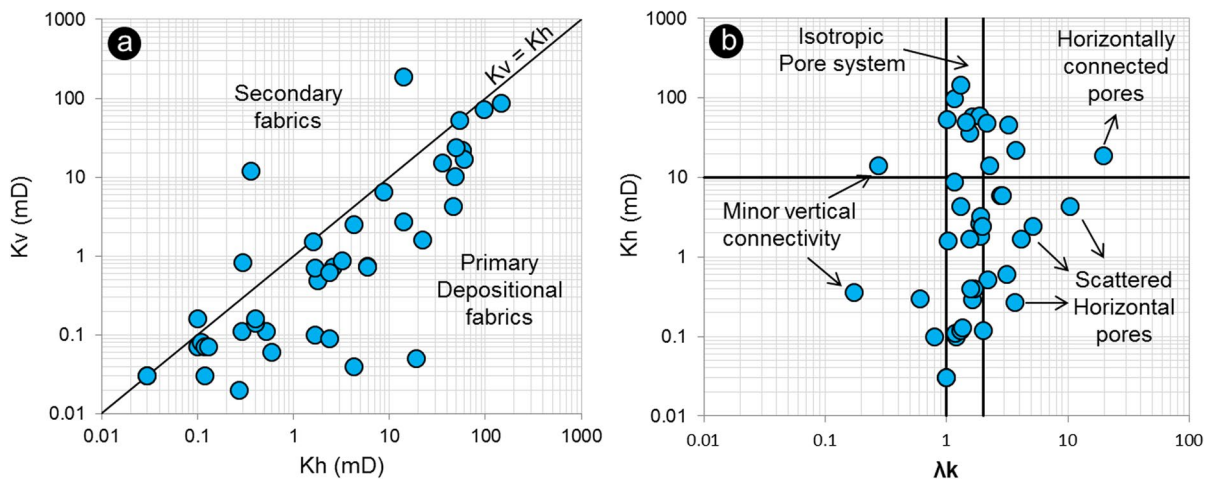
Fig. 12 Relationship between **a** horizontal permeability (Kh) and vertical permeability (Kv), **b** permeability anisotropy (λk) and Kh, from Matulla sandstone reservoir from the well A-3

porosity and permeability of Matulla sandstone are higher in the well G-11 (2 μm < R35 < 10 μm, megaporous) than well A-3. The Wata samples, in comparison, exhibit 21.3–25.6% porosity and 63.7–412 mD permeability indicating macro- to megaporosity (Fig. 11).

Vertical permeability measurements were available only for Matulla reservoir from the well A-3, which ranges between 0.02 and 185 mD (Fig. 12a). Most of the measurements indicate Kv/Kh < 1 representing predominantly primary depositional fabric over secondary fabrics (Fig. 12a). A cross plot between horizontal permeability and permeability anisotropy is presented in Fig. 12b (Leila et al. 2023). Permeability anisotropy of the Matulla sandstones range between 0.17 and 19.5, however majority of the data distribution indicates 1 < λk < 2, indicating dominantly isotropic pore system (Fig. 12b). Certain degree of horizontal pore communication (scattered or connected)

is also observed with minor vertical pore connectivity. Such inferences could not be made on Wata reservoir due to the unavailability of Kv measurements in any of the wells. Statistical summary of the core-measured porosity and permeability of the two studied sandstone reservoirs is presented in Table 1. A higher CV (coefficient of variation) value is indicative of wider data distribution, as has been the case in the Matulla porosity and permeability measurements, especially from the well A3.

4.2.2 Wireline log analysis

Wireline log-based petrophysical assessment was utilized to quantify the reservoir properties of the Matulla and Wata sandstones. The analysis involves the estimation of key petrophysical properties and net pay thickness. The results from three of the studied wells are presented in Figs. 15, 16, 17 and 18.

Table 1 Statistical summary of the core-measured porosity, horizontal and vertical permeability of the Matulla (52 samples) and Wata (6 samples) sandstone reservoirs from the three cored wells. 'Avg' and 'CV' denote the average values and coefficient of variation

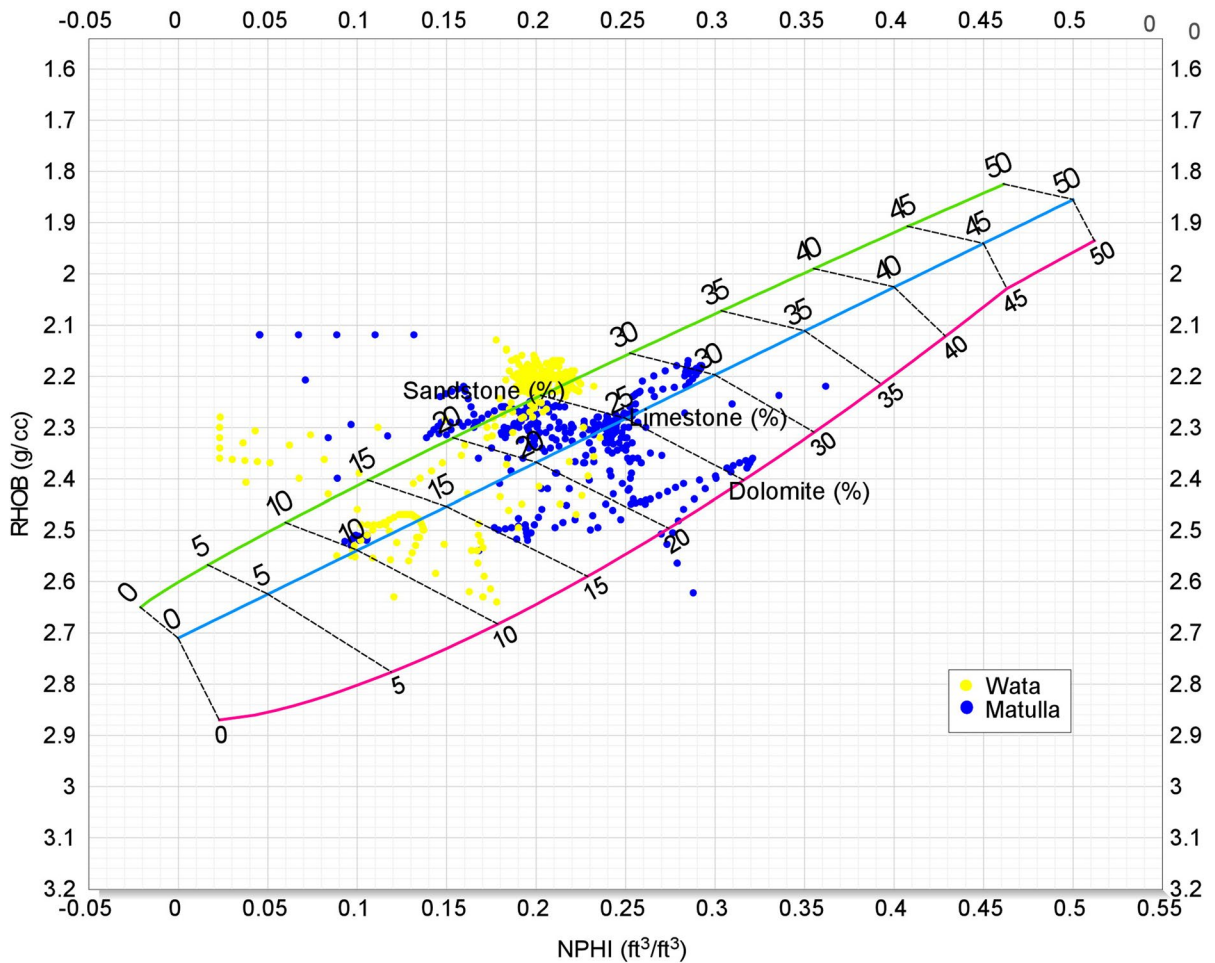| Core-measured Petrophysical properties	Matulla (Wells A3 and G11)				Wata (Wells A10 and G11)			
	Min	Max	Avg	CV	Min	Max	Avg	CV
Porosity (%)	4.5	27.1	17.82	0.34	21.3	25.6	23.25	0.08
Kh (mD)	0.03	1490	78.96	3.66	63.7	412	160.37	0.7942
Kv (mD)	0.02	185	11.89	2.73	–	–	–	–

Fig. 13 Cross-plot between bulk-density and neutron porosity of the Matulla and Wata Formations (including the reservoir pay zones) indicating the lithological composition, from the well A-10

To characterize the lithologies, we generated the cross-plots between bulk-density and neutron porosity (Fig. 13) and matrix density vs. matrix slowness (Fig. 14). Both the studied formations exhibit the influence of carbonates. It is to be noted that pore-filling carbonate cements were observed in the thin sections as well as SEM images, which corroborates well with the observations from the mentioned cross-plots. For estimating Sw, we have utilized $a = 1$, $m = 2$, $n = 2$ and Rw = 0.03 ohmm. It is to be noted that using default input parameter values in Sw calculation and constant Rw regardless of change in the formation temperature may introduce uncertainties in the Sw estimation.

The core-measured porosity available from routine core analysis of three wells (A-3, A-10, and G-11)

were plotted along with the petrophysical composite plots (Figs. 15, 16, 17) which correlates well with the log-based porosity (Φt) estimations. Matulla Formation exhibits a lower average shale volume, higher effective porosity, and Sw in the well A-10 than G-11, thus contributing to higher net pay thickness based on the utilized petrophysical cut-offs. Key observation from the Matulla Formation of the well A-10 is that Matulla hosts two potential pay zones in the upper ($0.1 < \Phi t < 0.22$, Sw ~ 0.4 v/v, $0.1 > BVW > 0.06$) and lower ($0.1 < \Phi t < 0.25$, $0.3 > Sw > 0.1$, $BVW < 0.06$) intervals (Figs. 15, 16, 17), which were also observed in the well G-11. The middle Matulla in G-11 also consists of pay intervals with $0.1 < Vsh < 0.3$, $0.2 < \Phi t < 0.3$, $0.5 > Sw > 0.2$, $0.12 > BVW > 0.06$ (Figs. 15, 16, 17); the same correlated interval in the
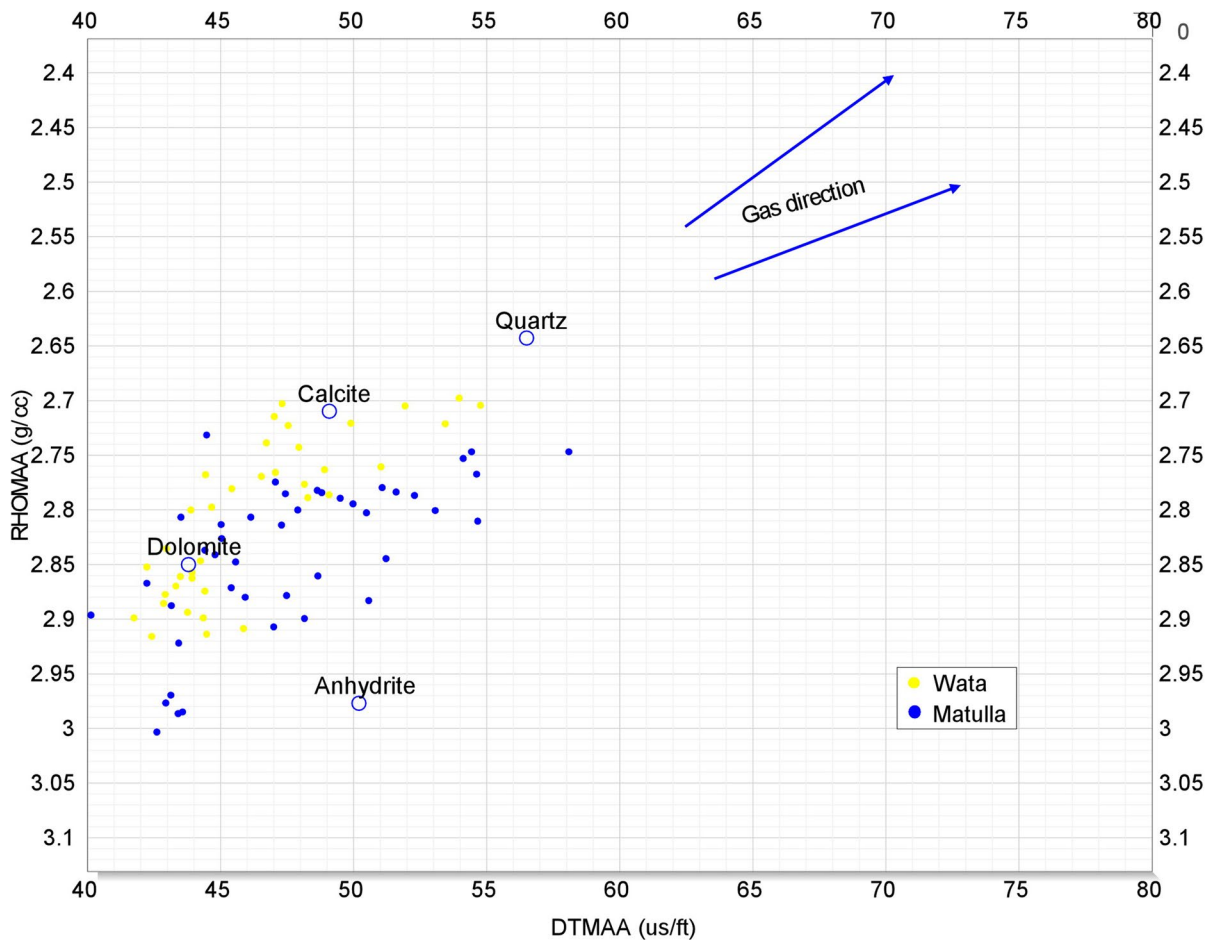
Fig. 14 Cross-plot between matrix density (RHOMAA) and matrix slowness (DTMAA) (Schlumberger 1972) of the Matulla and Wata Formations from the well B-6 indicating the effect of calcareous matrix within the studied reservoirs

well A-10 exhibits Sw > 0.5 v/v, therefore not inferred as pay zone (Figs. 15, 16, 17).

The Wata Formation from the well A-10 (Fig. 18) exhibits a very consistent clean GR (< 30 api), high resistivity (~ 200 ohmm) zone with density-neutron porosity cross over in the lower interval. This interval exhibits 30 > Vsh > 5, Φt up to 0.25 v/v, and 0.25 > Sw > 0.20, and a 65 ft of net pay is inferred.

4.3 Gas chromatography

Mudlogging data was analysed from the well A-10, where Matulla and Wata pay zones are inferred based on petrophysical cut offs. Calculated wetness (Wh) varies between 17.5 and 40, which indicates the presence of oil (Fig. 19) along with Ch < 0.5. In the

Matulla pay zones, Bh ≥ Wh due higher C1 and C2 peaks, while Wata reservoir exhibits good separation between Wh and Bh. Usually, Bh < < Wh indicates the possibility of residual oil, which is not the case for the studied reservoirs here (Fig. 19). We utilized C1/C2 ratio as a quick look indicator. The Matulla pay zones indicate C1/C2 varying between 3 and 7, which suggests the presence of low gravity (10–15 API) to medium gravity oil (15–35 API). The Wata pay zone indicates C1/C2 ~ 10.74 in the top part, which is indicative of gas, then it decreases to < 10, i.e., oil zone (Fig. 19). This may indicate a gas-oil contact within Wata. This observation is also supported by that fact that Ch > 0.5 in the top part of the Wata pays which indicates high GOR oil. However, such fluid contacts need to be confirmed by formation
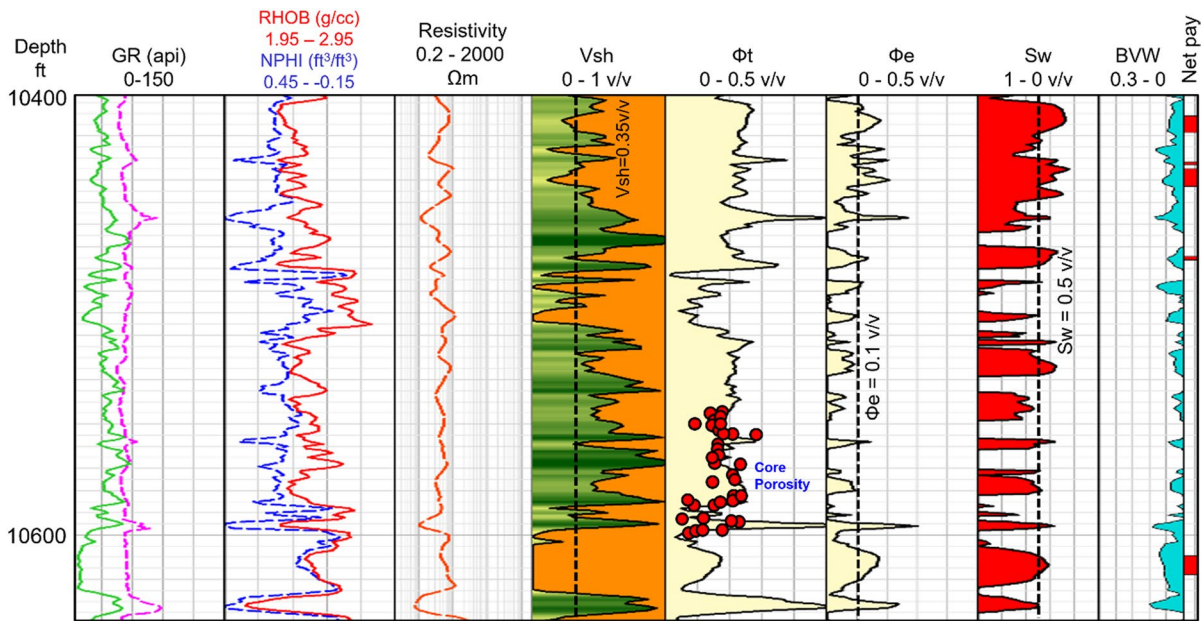
Fig. 15 Petrophysical interpretation of the Matulla Formation from the well A-3 indicating key petrophysical properties assessed from wireline logs (GR = gamma ray, RHOB = bulk-density, NPHI = neutron porosity). Red dots on the Total porosity (Φt) track represent the measurements from routine core analysis in the Matulla interval in A-3

pressure measurements and change in fluid gradients, which were unfortunately not recorded in the studied wells. Since both the reservoir zones exhibit C1/C4 ratio higher than C1/C3 ratio, we infer that the studied reservoirs are not water wet (Fig. 19).

5 Discussions

5.1 Comments on depositional environment

The pre-rift sediments of the Gulf of Suez Basin were deposited in continental margin sags. The first subsidence cycle deposited clastic Nubia Formation during Carboniferous-Lower Cretaceous period, while the second subsidence cycle commenced from Upper Cretaceous and deposited mixed siliciclastic-carbonate sediments (Atia et al. 2015). Hassouba et al. (1992) reported shallow marine origin of the Matulla and Wata formations. Based on the palyno-facies assemblages, El Diasty et al. (2014) inferred that Matulla sediments were deposited in a shelf setting, possibly near the shorelines. El-Azabi and El-Araby (2007) interpreted the primary sedimentary structures and architectural elements of the Matulla

interval and interpreted that the Matulla clastic facies were deposited in a foreshore-shoreface to shallow subtidal environment under the influence of variable wave energy conditions. Kassem (2018) inferred lower intertidal to slightly deep subtidal settings for Matulla sandstones and deciphered that the main oil reservoir of lower Matulla consists of a tidal channel. In a recent work, Kassem et al. (2022) presented a microfacies analysis of the Wata Formation and inferred an intertidal/shelf depositional setting. The fine to very fine-grained sandstones of the studied Matulla and Wata reservoirs include glauconites, as seen in the thin sections (Figs. 5a, 5d, 7b). Glauconites are widely reported from Cretaceous marine sediments deposited in a warm climate (Banerjee et al. 2016). There are many reported examples of glauconitic sandstones from Egypt which were deposited in a shoreface-shallow shelf environment during Tethys transgression which had occurred during Cretaceous (Said 1990; Catuneanu et al. 2006; Khalifa and Catuneanu 2008; Baioumy and Boulis 2012). Glauconites are also reported from the Matulla sandstones from the nearby July oil field (Ali et al. 2022). Based on the petrographic observations, a shallow marine
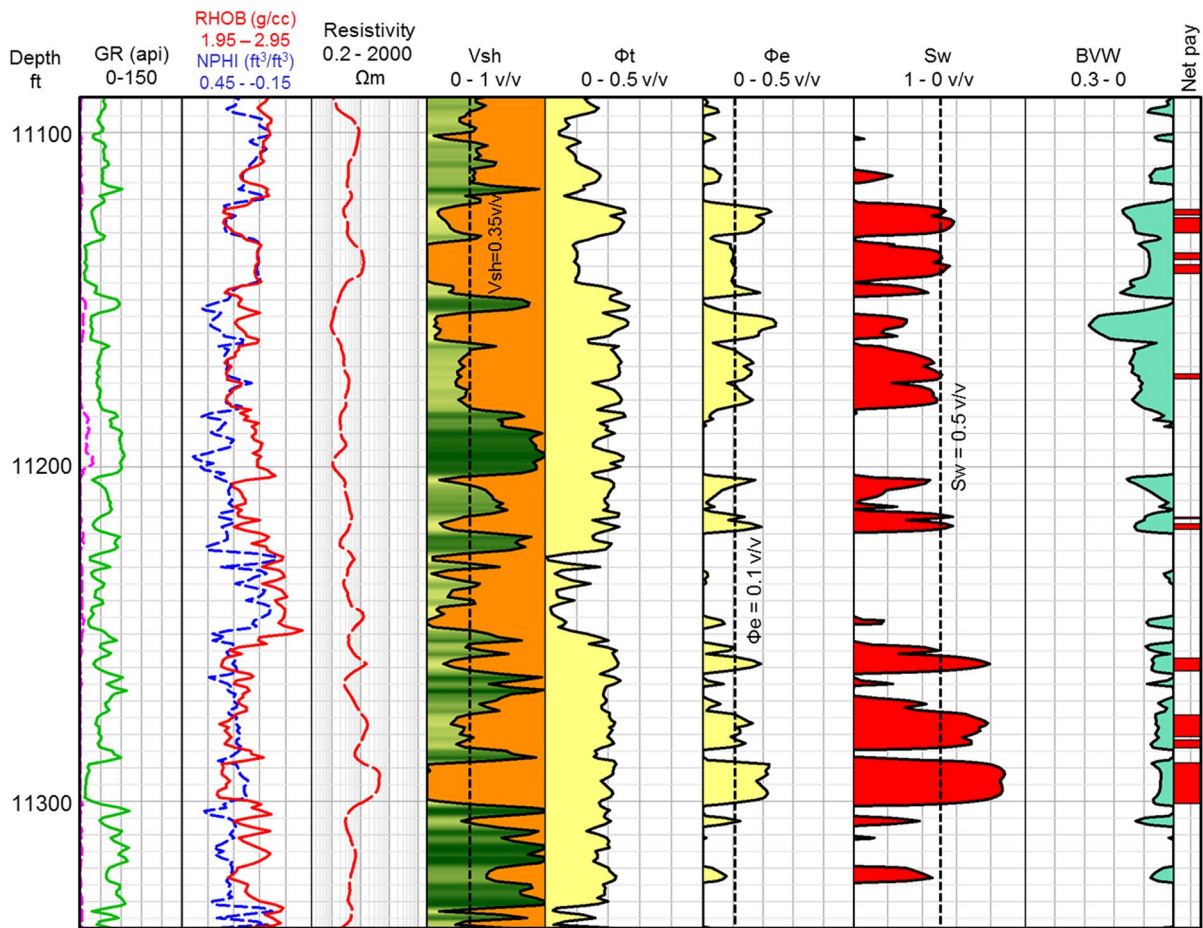
Fig. 16 Petrophysical interpretation of the Matulla Formation from the well A-10 indicating key petrophysical properties assessed from wireline logs (GR = gamma ray, RHOB = bulk-density, NPHI = neutron porosity)

depositional environment is assigned to the studied reservoirs, which corroborates with the findings of previous researchers from other parts of the Gulf of Suez Basin.

5.2 Diagenetic factors

Thin section and SEM analyses indicate that the studied Matulla and Wata reservoirs have been largely affected by diagenetic alterations. The early diagenetic changes include clay infiltration (Figs. 5a, 7b–d), quartz overgrowth cements and pressure solution among quartz grains (Figs. 5a–c, 7a–c). Later stage of diagenesis resulted in extensive leaching and dissolution of feldspar grains (Figs. 5c, 7c, 8a), chloritized alteration rims surrounding quartz grains (Figs. 7d, 8b), calcite cementation (Figs. 5d, 6d,

7b) and kaolinite precipitation (Figs. 5, 6c, d, 7a, d, 8b–d). Pyrites formed at much later stage (Fig. 5a, d). Concavo-convex grain boundaries and point to point boundaries along with grain to grain pressure solutions resulted in a slightly inhomogeneous packing of framework grains, which indicate variable degrees of compaction affecting the two studied reservoirs.

Cementation can have a tremendous negative effect on reservoir quality. Worden and Morad (2000) reported loss of almost half of the original rock porosity due to cementation. Both the reservoirs indicated certain degree of calcite cementation (Figs. 5d, 6d, 7b); however not observed in every sample. XRD indicates 0.5–5% calcite in Matulla and Wata reservoirs. Thin sections and SEM indicate kaolinite is the most prominent clay mineral phase present in both the reservoirs. Kaolinite is
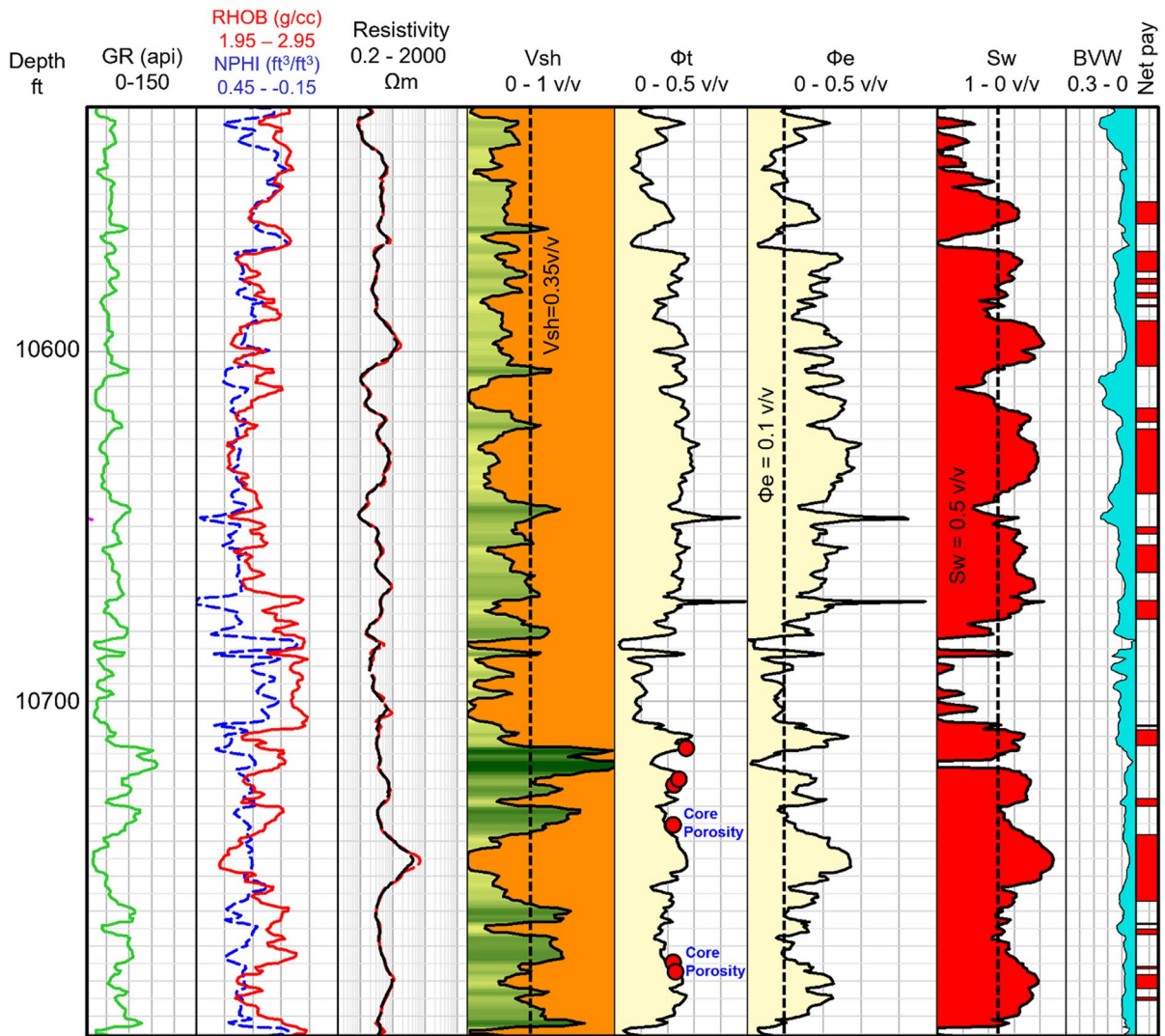
Fig. 17 Petrophysical interpretation of the Matulla Formation from the well G-11 indicating key petrophysical properties assessed from wireline logs (GR = gamma ray, RHOB = bulk-density, NPHI = neutron porosity). Red dots on the Total porosity (Φt) track represent the six measurements from routine core analysis in the Matulla interval in G-11

observed in all the samples in the form of booklets filling the pore spaces (Figs. 5, 6c, d, 7a, d, 8b–d). Cao et al. (2017) inferred that kaolinites commonly occur because of feldspar dissolution in warm and humid climatic conditions. Chlorites were not seen in Matulla samples; however, it occurs as coatings surrounding quartz grains (Fig. 7d) which generally forms in the early diagenesis (Dowey et al. 2012; Freiburg et al. 2016) and favoured by the presence of iron-rich clays (Zhu et al. 2017). Such chlorite rims reduce surface area for further quartz cementation

and stops overgrowth, thus helps in porosity preservation (Nguyen et al. 2013; Hansen et al. 2017). Clay pseudomatrix is commonly observed in all the samples from Matulla and Wata, which results from the compaction/alteration of argillaceous rock fragments. Some detrital clay is suspected as matrix due to the finely laminated texture of the rock, but it is often difficult to distinguish from pseudomatrix.

Primary intergranular porosity is dominant, while feldspar dissolution contributed to secondary porosity. Dissolution has been observed along the feldspar
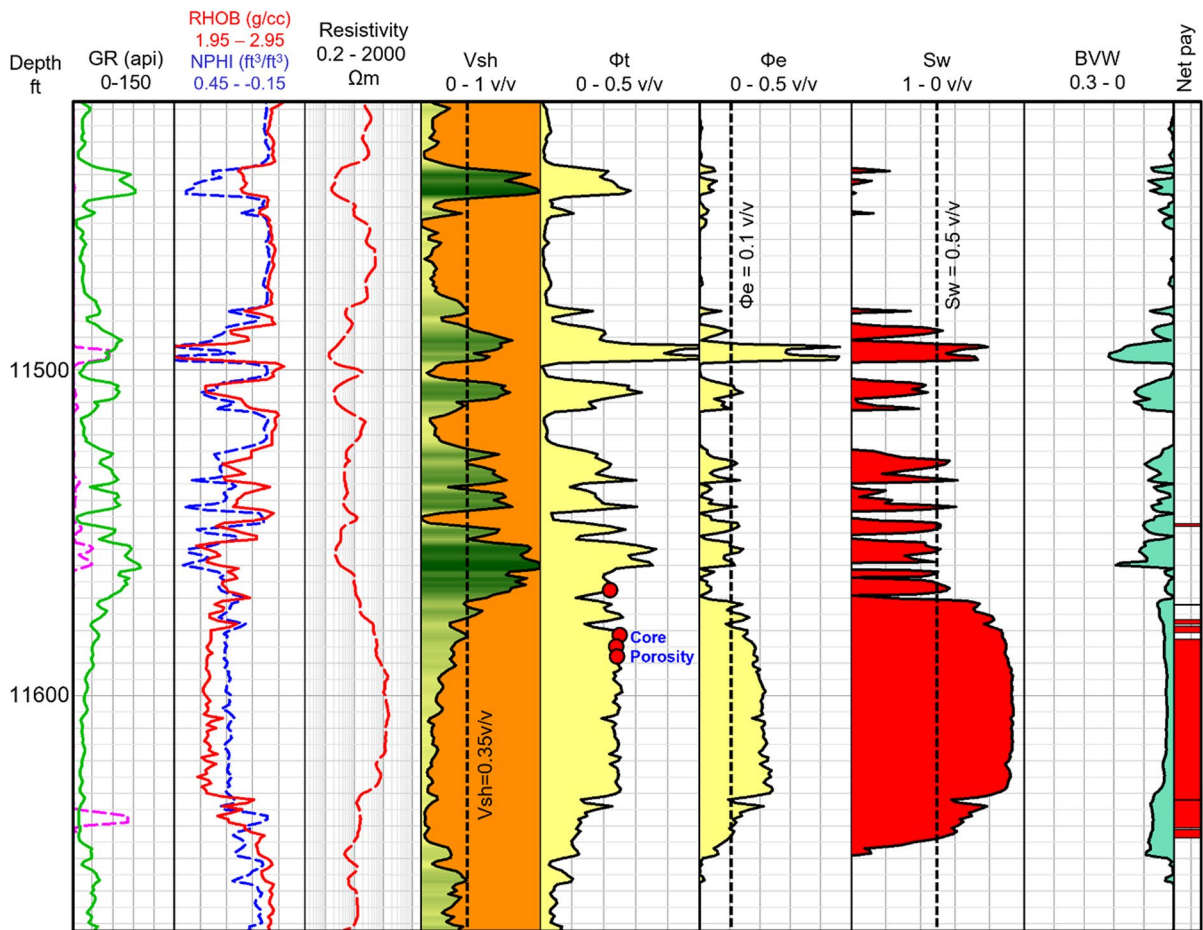
Fig. 18 Petrophysical interpretation of the Wata Formation from the well A-10 indicating key petrophysical properties assessed from wireline logs (GR = gamma ray, RHOB = bulk-density, NPHI = neutron porosity). Red dots on the Total porosity (Φt) track represent the four measurements from routine core analysis in the Wata interval in A-10

cleavage planes (Fig. 8a) and inferred as reservoir quality enhancing diagenetic agent. With increase in overburden burial and temperature, feldspar becomes chemically unstable (Ma et al. 2017) and can experience dissolution due to its interaction with low pH meteoric water (Zhang et al. 2018).

5.3 Inferences on reservoir petrophysical properties

Reservoir storage capacity and flow potential directly affects the production scenario, economics, and field development strategies. The studied Matulla and Wata reservoirs predominantly consist of primary intergranular porosity, as seen in all the thin sections. All samples have good, interconnected pores, but varying pore-throat sizes based on packing and grain-size

distribution. Diagenesis has critical effects on the reservoir quality, i.e., it can significantly enhance or diminish reservoir qualities. This study identifies dissolution as a porosity enhancing factor. Secondary pores, such as grain moulds and "honey-comb" micropores, are the result of dissolution of unstable feldspar grains. At the same time clay infiltration, silica and calcite cementation occurred as contributed to porosity reduction. Majority of the feldspar grains of both the reservoirs are observed to be affected by dissolution. Cross plots between total feldspar content (from XRD) and core-measured porosity (Fig. 20a) and permeability (Fig. 21a) indicate that these increase with the increase in feldspar content within Matulla and Wata reservoirs. Figures 20b and 21b
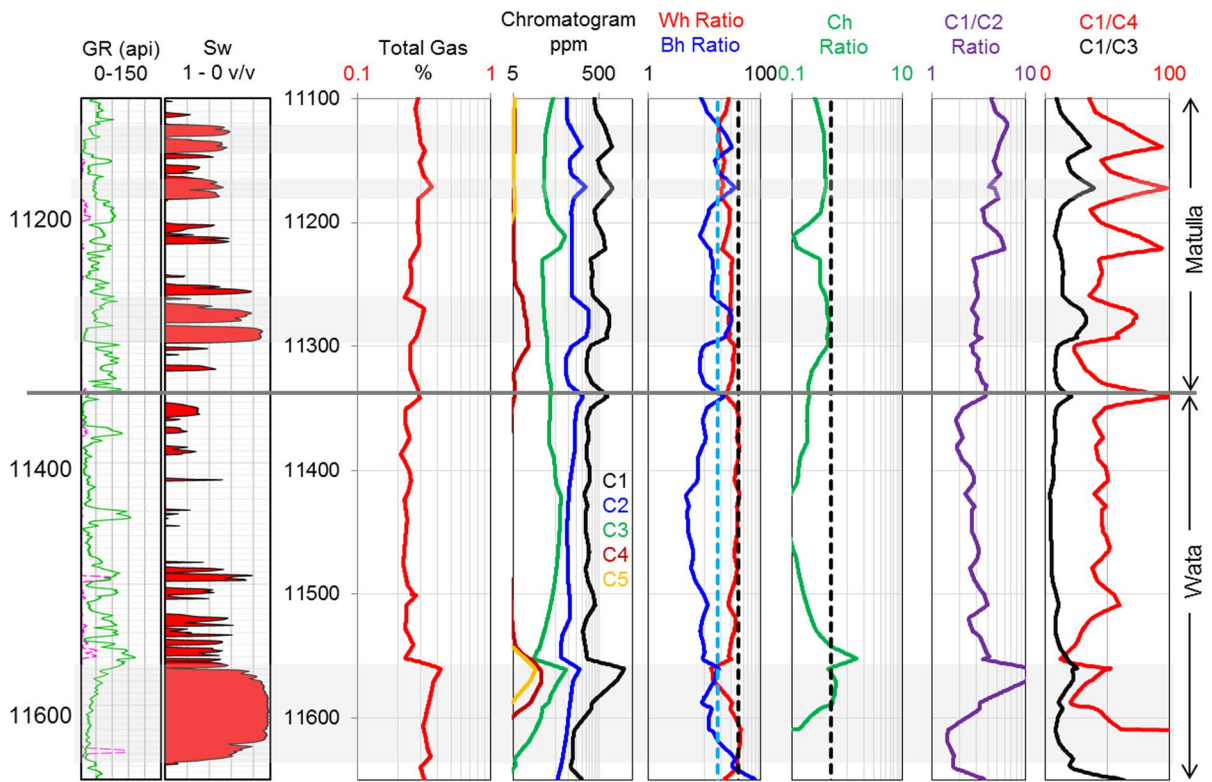
Fig. 19 Gas analysis of the Matulla and Wata Formations, well A-10 using the chromatograph data [Wh = wetness, Bh = balance, Ch = character ratio]. Grey shaded intervals indicate the net pay zones based on petrophysical cut offs
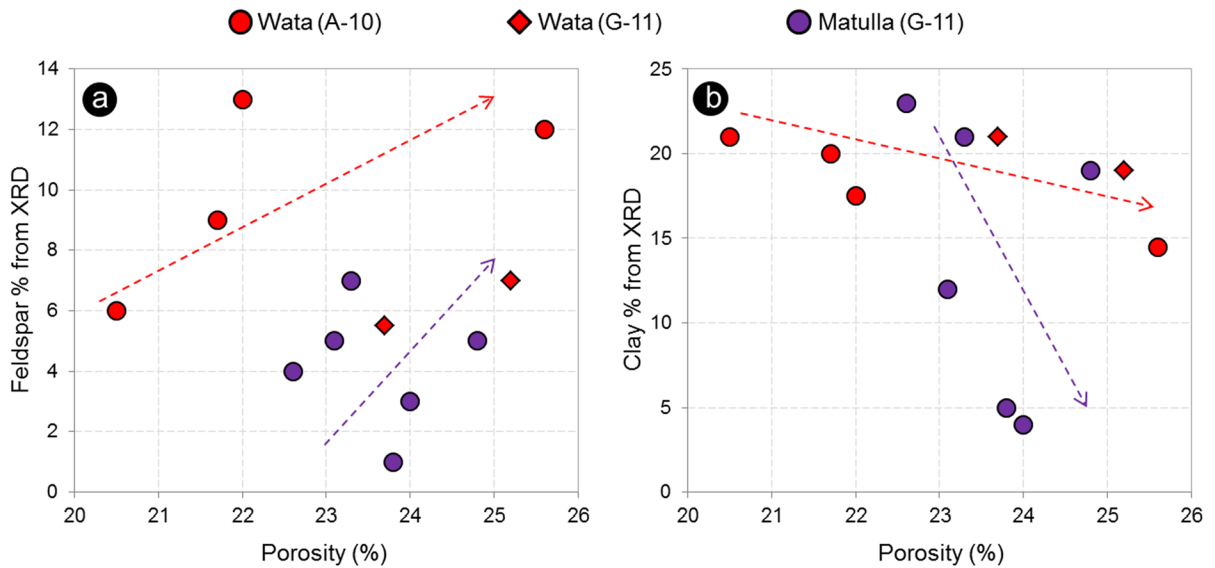

Fig. 20 Effect of **a** feldspar (dissolution) and **b** clay content on reservoir porosity
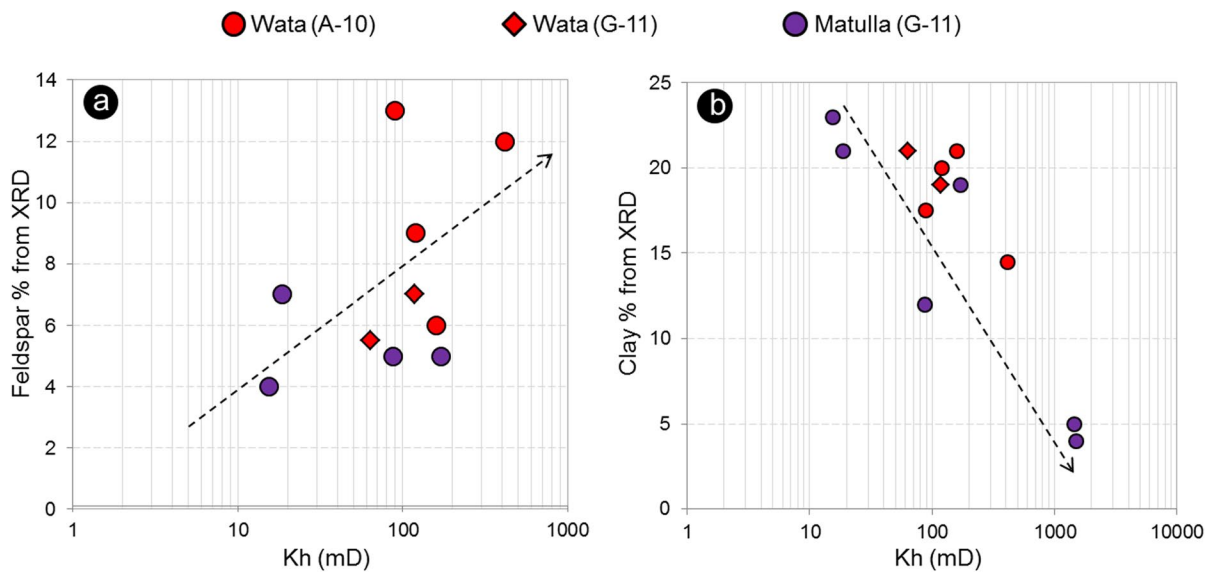
Fig. 21 Effect of **a** feldspar (dissolution) and **b** clay content on reservoir permeability

represent the negative effect of pore-filling clay on reservoir porosity and permeability.

In general, the Wata Formation shows higher hydrocarbon saturation when compared with the Matulla interval. However, Matulla Formation hosts multiple pay intervals when compared to Wata. The Matulla contributed to net pay in the well G-11 but exhibited higher water saturation in the well A-10. Also, to be noted that, the studied formations exhibit large thickness variations in these wells indicating high heterogeneity vertically as well as laterally. The absence of the Wata Formation in the well A3 is contributed by the faults or tectonic uplift, where we encountered Raha Formation right below the Matulla interval. This indicates lateral variability within Matulla and Wata. Similar observations were also reported by El-Ghamri et al. (2002) who inferred that the Matulla and Wata sandstones have high lateral and vertical heterogeneity in terms of continuity, thickness, and oil–water boundary.

6 Conclusions

Based on the integrated analysis using the petrographic thin sections, SEM, XRD, routine core analysis, gas chromatography, and wireline logs, we have assessed the reservoir characteristics of the Matulla and Wata clastic reservoirs from the October field. Our conclusions are summarised as below:

- The analysed sandstones of the Matulla and Wata reservoirs are inferred as glauconite-bearing subarkose quartz arenites. The general composition of each sample is very similar with only subtle differences in relative percentages of feldspars, argillaceous rock fragments, clayey pseudomatrix, and/or calcite cement.
- These changes correspond with the overall rock texture/fabric, in that with increasing planar lamina, there is a general increase in the pseudomatrix content of the rock. The feldspathic and lithic content of the sands is thought to be slightly lower than the original content due to the dissolution and partial dissolution of many of these unstable constituents.
- Gas chromatography and wireline log-based quantitative petrophysical assessment indicates that the Matulla and Wata sandstones are oil bearing reservoirs with high vertical and lateral heterogeneities in net pay distribution.
- The meso-megaporous reservoirs are dominated by primary intergranular porosity along with the secondary porosity contribution by feldspar dissolution. Clay infiltration and carbonate cementation reduced the reservoir qualities to a certain

degree but overall, both the reservoirs exhibit excellent properties.

Availability of data and materials   The geophysical data in the present work is confidential.

Declarations

Ethics approval and consent to participate   We certify that this manuscript reflects our own research and has never been published before and not being considered for publication anywhere.

Consent to publish   Here, we give our consent for the present manuscript to be published in this journal after the acceptance.

Competing interests   Here, we authorize that there is no conflict of interest.

References

Abdine S, Homossani A, Lelek J (1992) October Field: the latest giant under development in the Gulf of Suez. Geology of the Arab World, Cairo University, pp 61–86

Ali AM, Radwan AE, Abd El-Gawad EA, Abdel-Latief A-SA (2022) 3D integrated structural, facies and petrophysical static modeling approach for complex sandstone reservoirs: a case study from the Coniacian-Santonian Matulla formation, July Oilfield, Gulf of Suez, Egypt. Nat Resour Res 31(1):385–413

Alsharhan AS (2003) Petroleum geology and potential hydrocarbon plays in the Gulf of Suez rift basin, Egypt. Rev Am Assoc Petrol Geologists Bull 87(1):143–180

Askar M, Abdallah A, Gad I (2020) Downhole scales associated with October Field formation waters and water injection using a shallow aquifer. In: SPE International conference and exhibition on formation damage control, Lafayette, Louisiana, USA, Feb 19–21. SPE-199300.

Asquith G, Gibson C (1982) Basic well log analysis for geologists: methods in Exploration series. AAPG, Tulsa, Oklahoma.

Atia HM, Ahmed MA, Korrat I (2015) Thermal maturation simulation and hydrocarbon generation of the Turonian Wata Formation in Ras Budran oil field, Gulf of Suez, Egypt. J Enviro Sci 44(1):57–92

El Bahr M, Patchett JG, Wiley R (1992) Modeling the effects of glauconite on some openhole logs from the Lower Senonian in Egypt. In: 11th EGPC Petroleum exploration and production conference, 1, 494–514

Baioumy H, Boulis S (2012) Glauconites from the Bahariya oasis: an evidence for cenomanian marine transgression in Egypt. J Afr Earth Sc 70:1–7

Banerjee S, Bansal U, Thorat AV (2016) A review on paleogeographic implications and temporal variation in glaucony composition. J Palaeogeogr 5(1):43–71

Barakat MK, El-Gendy NH, EL-Shishtawy AM, Shawaf FM (2022) Application of well log analysis to estimate the petrophysical parameters of the Lower Rudeis Formation in July Oilfield, Gulf of Suez, Egypt. Al-Azhar Bull Sci 33(2D):127–143

Borling DC, Powers BS, Ramadan N (1996) Water shut-off case history using through-tubing bridge plugs; October field, Nubia Formation, Gulf of Suez, Egypt. In Abu Dhabi International Petroleum Exhibition and Conference, Abu Dhabi, United Arab Emirates, Oct 13–16. SPE-36213

Bosworth W, Khalil SM, Ligi M, Stockli DF, McClay KR (2020) Geology of Egypt: The Northern Red Sea. The geology of Egypt. Springer, Cham, pp 343–374

Buckles RS (1965) Correlating and averaging connate water saturation data. J Can Pet Technol 4(1):42–52

Cao B, Luo X, Zhang L, Sui F, Lin H, Lei Y (2017) Diagenetic evolution of deep sandstones and multiple-stage oil entrapment: a case study from the Lower Jurassic Sangonghe Formation in the Fukang Sag, Central Junggar basin (NW China). J Petrol Sci Eng 152:136–155

Catuneanu O, Khalifa MA, Wanas HA (2006) Sequence stratigraphy of the lower cenomanian Bahariya Formation, Bahariya oasis, Western Desert, Egypt. Sedim Geol 190:121–137

Dott RH (1964) Wacke, graywacke and matrix; what approach to immature sandstone classification? J Sedim Res 34(3):625–632

Dowey PJ, Hodgson DM, Worden RH (2012) Pre-requisites, processes, and prediction of chlorite grain coatings in petroleum reservoirs: a review of subsurface examples. Mar Petrol Geol 32:63–75

EGPC (1996) Gulf of Suez oil fields (a comprehensive overview): Egyptian General Petroleum Corporation, Cairo, p 736

El Sharawy MS, Nabawy BS (2016) Geological and petrophysical characterization of the Lower Senonian Matulla Formation in Southern and Central Gulf of Suez, Egypt. Arab J Sci Eng 41:281–300

El Diasty WS, El Beialy SY, Abo Ghonaim AA, Mostafa AR, El Atfy H (2014) Palynology, palynofacies and petroleum potential of the Upper Cretaceous-Eocene Matulla, Brown Limestone and Thebes formations, Belayim oilfields, central Gulf of Suez, Egypt. J African Earth Sci 95:155–167

El Diasty WS, El Beialy SY, Mostafa AR, Abo Ghonaim AA, Peters KE (2020) Chemometric differentiation of oil families and their potential source rocks in the Gulf of Suez. Nat Resour Res 29(3):2063–2102

El-Azabi MH, El-Araby A (2007) Depositional framework and sequence stratigraphic aspects of the Coniacian-Santonian mixed siliciclastic/carbonate Matulla sediments in Nezzazat and Ekma blocks, Gulf of Suez, Egypt. J African Earth Sci 47:179–202

El-Gendy N, Barakat M, Abdallah H (2017a) Reservoir assessment of the Nubian sandstone reservoir in South Central Gulf of Suez Egypt. J Afr Earth Sc 129:596–609

El-Gendy NH, El-Shishtawy A, Barakat MKh, Shawaf FM (2017b) Applying sedimentological and geophysical techniques for facies analysis and depositional history of July Member sandstones, the northern area of July oilfield, Gulf of Suez, Egypt. J Appl Geol Geophys (IOSR-JAGG) 5(1):84–106

El-Gendy NH, Radwan AA, Waziry M, Dodd TJ, Barakat MKh (2022) An integrated sedimentological, rock typing, image logs and artificial neural networks analysis for reservoir quality assessment of the heterogenous fluvial-deltaic Messinian Abu Madi reservoirs, Salma field, onshore East Nile Delta, Egypt. Marine Petrol Geol 145:105910

El-Ghamri MA, Warburton IC, Burley SD (2002) Hydrocarbon generation and charging in the October Field, Gulf of Suez, Egypt. J Petrol Geol 25(4):433–464

ENI (2019) New resources discovered in the Gulf of Suez offshore Egypt. In: Natural Resources, Press release, Oct 25. https://www.eni.com/en-IT/media/press-release/2019/10/eni-new-resources-discovered-in-the-gulf-of-suez-offshore-egypt.html

Farouk S (2015) Upper Cretaceous sequence stratigraphy of the Galala Plateaux, western side of the Gulf of Suez, Egypt. Mar Petrol Geol 60:136–158

Lelek JJ, Shepherd DB, Stone DM, Abdine AS (1992) October Field—the latest giant under development in Egypt's Gulf of Suez. In M. T. Halbouty (Ed.), Giant Oil and Gas Fields of the Decade 1978–1988. AAPG Memoir, 54:231–249

Freiburg JT, Ritzi RW, Kehoe KS (2016) Depositional and diagenetic controls on anomalously high porosity within a deeply buried CO_2, storage reservoir—the Cambrian Mt. Simon sandstone, Illinois basin, USA. Int J Greenh Gas Control 55:42–54

Gawad EA, Fathy M, Reda M, Ewida H (2021a) Petroleum geology: 3D reservoir modelling in the central Gulf of Suez, Egypt, to estimate the hydrocarbon possibility via petrophysical analysis and seismic data interpretation. Geol J 56(10):5329–5342

Gawad EA, Fathy M, Reda M, Ewida H (2021b) Source rock evaluation of the Central Gulf of Suez, Egypt: A 1D basin modelling and petroleum system analysis. Geol J 56(7):3850–3867

Hansen HN, Løvstad K, Müller R, Jahren J (2017) Clay coating preserving high porosities in deeply buried intervals of the Stø formation. Mar Petrol Geol 88:648–658

Hasouba M, Abd El Shafy A, Mohamed A (1992) Nezzazat Group-reservoir geometry and rock types in the October field area, Gulf of Suez. In: 11th EGPC petroleum exploration and production conference, 1, pp 293–317

Hassan NR, Rocha G, Michel CM, Hey M-JV (2006) Donwhole integrity management in October field, Gulf of Suez, Egypt. In: SPE Abu Dhabi international petroleum exhibition and conference, Abu Dhabi, UAE, Nov 5–8. SPE-100600

Haworth JH, Sellens M, Whittaker A (1985) Interpretation of hydrocarbon shows using light (C1–C5) hydrocarbon gases from mud-log data. Am Assoc Petrol Geol (AAPG) Bull 69(8):1305–1310

Hempton MR (1987) Constraints on Arabian plate motion and extensional history of the Red Sea. Tectonics 6(6):687–705

Ibrahim AA, Mostafa A (1999) Production logging problem description in October field, Gulf of Suez. SPE Annual Technical Conference and Exhibition, Houston, Texas, Oct 3–6. SPE 56650

Ibrahim MM, Styler JW, Shamma HL, Elsherif MA, AboElalla EM (2008) Environmentally friendly and economic waterflood system for October Field at Gulf of Suez, Egypt. In: Indian oil and gas technical conference and Exhibition, Mumbai, India, Mar 4–6. SPE-112311-MS

Jackson CA, Gawthorpe RL, Sharp IR (2006) Style and sequence of deformation during extensional fault-propagation folding: examples from the Hammam Faraun and El-Qaa fault blocks, Suez Rift, Egypt. J Struct Geol 28:519–535

JPT (Journal of Petroleum Technology), (2022) Dragon Finds Oil in Gulf of Suez-New discovery could hold 100 million barrels of oil. In: Exploration/Discoveris, April 1. https://jpt.spe.org/dragon-finds-oil-in-gulf-of-suez

Kassem AA, Sharaf LM, Baghdady AR, El-Naby AA (2020) Cenomanian/Turonian oceanic anoxic event 2 in October oil field, central Gulf of Suez, Egypt. J African Earth Sci 165:103817

Kassem AA, Sen S, Radwan AE, Abdelghany WK, Abioui M (2021) Effect of depletion and fluid injection in the mesozoic and paleozoic sandstone reservoirs of the October Oil Field, Central Gulf of Suez Basin: implications on drilling, production and reservoir stability. Nat Resour Res 30:2587–2606

Kassem AA, Osman OA, Nabawy BS, Baghdady AR, Shehata AA (2022) Microfacies analysis and reservoir discrimination of channelized carbonate platform systems: an example from the Turonian Wata Formation, Gulf of Suez, Egypt. J Petrol Sci Eng 212:110272

Kassem A (2018) Diagenetic history and its effect on reservoir quality and reservoir characterization of sandstone sequences of Matulla Formation, October Field, Gulf of Suez, Egypt. International Conference and Exhibition,

Cape Town, South Africa, November 4–7. Search and Discovery Article #20452.

Khalifa MA, Catuneanu O (2008) Sedimentology of the fluvial and fluvio-marine facies of the Bahariya Formation (early Cenomanian), Bahariya oasis, Western Desert, Egypt. J African Earth Sci 55:89–103

Kolodzie S (1980) Analysis of pore throat size and use of the Waxman–Smits equation to determine OOIP in Spindle Field, Colorado. In: Proceedings society of petroleum engineers 55th annual technical fall conference. SPE-9382

LaBrecque JL, Zitellini N (1985) Continuous sea-floor spreading in Red Sea: an alternative interpretation of magnetic anomaly pattern. AAPG Bull 69(4):513–524

Lashin A, Mogren S (2012) Total organic caron enrichment and source rock evaluation of the Lower Miocene rocks based on well logs: October oil field, Gulf of Suez-Egypt. Int J Geosci 3(4):683–695

Leila M, Sen S, Ganguli SS, Moscariello A, Abioui M (2023) Integrated petrographical and petrophysical evaluation for reservoir management of the Upper Miocene Qawasim sandstones in West Dikirnis, onshore Nile Delta, Egypt. Geoenergy Sci Eng 226:211789

Ma B, Cao Y, Jia Y (2017) Feldspar dissolution with implications for reservoir quality in tight gas sandstones: evidence from the Eocene Es4 interval, Dongying depression, Bohai Bay basin, China. J Petrol Sci Eng 150:74–84

Makris J, Henke CH (1992) Pull-apart evolution of the Red Sea. J Pet Geol 15:127–134

Martilla RK, El Bahr M (1994) Evaluation of a lithology complex reservoir (Nezzazat Group) in the Gulf of Suez. In: 12th EGPC Exploration and Production Conference, 2, 472–482

Meshref WM (1990) Tectonic framework. In: Said R (ed) The geology of Egypt. Balkema, Rotterdam, pp 113–155

Mode AW, Anyiam OA, Egbujie BC (2014) The application of chromatographic gas ratio analysis in reservoir fluid evaluation of "beta" field in the Congo basin. J Geol Soc India 84:303–310

Nabawy BS, Barakat MK (2017) Formation evaluation using conventional and special core analysis: Belayim Formation as a case study, Gulf of Suez, Egypt. Arab J Geosci 10(25):1–23

Nabawy BS, Lashin AA, Barakat MK (2022) Implementation of lithofacies and microfacies types on reservoir quality and heterogeneity of the Late Cretaceous Upper Bahariya Member in the Shurouk Field, Shoushan Basin, North Western Desert, Egypt. J Asian Earth Sci 224:105014

Nassar IS, Noureldien DM (2013) A case study from October Field: Modeling heterogeneity results in improved reservoir management. In: SPE Reservoir Characterization and Simulation Conference and Exhibition. Abu Dhabi, UAE, Sep 16–18. SPE 165939.

Nguyen BTT, Jones SJ, Goulty NR, Middleton AJ, Grant N, Ferguson A, Bowen L (2013) The role of fluid pressure and diagenetic cements for porosity preservation in Triassic fluvial reservoirs of the Central Graben. North Sea AAPG Bull 97(8):1273–1302

Noureldien DM, Nabil S (2016) GUPCO experience with giant fields: Case studies from Egypt. In: Abu Dhabi International Petroleum Exhibition and Conference (ADIPEC), Abu Dhabi, UAE, Nov 7–10. SPE-183556

Pickett GR (1973) Pattern recognition as a means of formation evaluation. The Log Analyst, 14(04). SPWLA-1973-vXIVn4a1.

Pierson RM (2017) The ELLA GRA Process—concepts and methods for the prediction of reservoir hydrocarbon type using ratios of gas chromatography C1-C5 gases. AAPG Rocky Mountain Section Meeting, Billings, Montana, June 25–28. Search and Discovery Article #42122

Poupon A, Leveaux J (1971) Evaluation of water saturation in shaly formations. The Log Analyst, 12(04), SPWLA-1971-vXIIn4a1

Said R (1990) The geology of Egypt. Elsevier, New York, p 734

Schlumberger (1972) Log interpretation, Vol. 1. Principles. New York, USA, p 112

Schutz KI (1994) Structure and stratigraphy of the Gulf of Suez, Egypt. In: Landon SM (ed) Interior rift basins. AAPG Memoirs, Tulsa, 59, 57–96.

Sercombe WJ, Golob BR, Kamel M, Stewart JW, Smith GW, Morse JD (1997) Significant structural reinterpretation of the subsalt, giant October Field, Gulf of Suez, Egypt, Using SCAT, isogon-based sections and maps, and 3-D seismic. Lead Edge 6(8):1089–1208

Sercombe WJ, Thurmon L, Morse J (2012) Advanced reservoir modeling i n poor seismic; October field, Northern Gulf of Suez, Egypt. In: AAPG International Conference and Exhibition, Milan, Oct 23–26. Search and Discovery Article # 40872

Wescott WA, Atta M, Dolson JC (2016) PS A brief history of the exploration history of the Gulf of Suez, Egypt.

Worden RH, Morad S (2000) Quartz cementation in oil field sandstones: a review of the key controversies. In: Worden RH, Morad S (eds) Quartz cementation in sandstones, vol 29. International Association of Sedimentologists (IAS) Special Publication, Oxford, pp 1–20

Zhang KX, Guo Y, Bai G, Wang Z, Fan B, Wu J, Niu X (2018) Pore structure characterization of the Eocene Sha-3 sandstones in the Bohai Bay Basin. China Energy Fuels 32(2):1579–1591

Zhu S, Wang X, Qin Y, Jia Y, Zhu X, Zhang J, Hu Y (2017) Occurrence and origin of pore-lining chlorite and its effectiveness on preserving porosity in sandstone of the Middle Yanchang Formation in the Southwest Ordos basin. Appl Clay Sci 148:25–38

Publisher's Note   Springer Nature remains neutral with regard to jurisdictional claims in published maps and institutional affiliations.